

1 **The Arabidopsis mitochondrial dicarboxylate carrier 2 maintains leaf metabolic**
2 **homeostasis by uniting malate import and citrate export**

3

4 Chun Pong Lee¹, Marlene Elsässer², Philippe Fuchs^{2,3}, Ricarda Fenske¹, Markus Schwarzländer²,
5 A. Harvey Millar^{1*}

6

7 ¹ ARC Centre of Excellence in Plant Energy Biology, Bayliss Building M316, University of Western
8 Australia, 35 Stirling Highway, Crawley 6009, Western Australia, Australia.

9 ² Institute of Plant Biology and Biotechnology, University of Münster, Schlossplatz 8, D-48143
10 Münster, Germany

11 ³ Institute of Crop Science and Resource Conservation, Rheinische Friedrich-Wilhelms-Universität
12 Bonn, Friedrich-Ebert-Allee 144, D-53113 Bonn, Germany

13

14

15 *Corresponding author: harvey.milllar@uwa.edu.au

16

17

18

19 **Keywords:** mitochondria, transport, malate, citrate, TCA cycle

20

21

22 **Author Contributions:** CPL performed most of the experiments in this manuscript and undertook data
23 analysis. ME and PF conducted experiments with Peredox-mCherry lines and carried out data analysis.
24 RF undertook MRM development and analysis. CPL, MS and AHM developed the experimental plan. CPL
25 and AHM wrote the manuscript and all authors revised the manuscript.

26

27 **ABSTRACT**

28 Malate is the major substrate for respiratory oxidative phosphorylation in illuminated leaves. In the
29 mitochondria malate is converted to citrate either for replenishing tricarboxylic acid (TCA) cycle with
30 carbon, or to be exported as substrate for cytosolic biosynthetic pathways or for storage in the
31 vacuole. In this study, we show that DIC2 functions as a mitochondrial malate/citrate carrier *in vivo* in
32 Arabidopsis. DIC2 knockout (*dic2-1*) results in growth retardation that can only be restored by
33 expressing DIC2 but not its closest homologs DIC1 or DIC3, indicating that their substrate preferences
34 are not identical. Malate uptake by non-energised *dic2-1* mitochondria is reduced but can be restored
35 in fully energised mitochondria by altering fumarate and pyruvate/oxaloacetate transport. A reduced
36 citrate export but an increased citrate accumulation in substrate-fed, energised *dic2-1* mitochondria
37 suggest that DIC2 facilitates the export of citrate from the matrix. Consistent with this, metabolic
38 defects in response to a sudden dark shift or prolonged darkness could be observed in *dic2-1* leaves,
39 including altered malate, citrate and 2-oxoglutarate utilisation. There was no alteration in TCA cycle
40 metabolite pools and NAD redox state at night; however, isotopic glucose tracing reveals a reduction
41 in citrate labelling in *dic2-1* which resulted in a diversion of flux towards glutamine, as well as the
42 removal of excess malate via asparagine and threonine synthesis. Overall, these observations
43 indicate that DIC2 is responsible *in vivo* for mitochondrial malate import and citrate export which
44 coordinate carbon metabolism between the mitochondrial matrix and the other cell compartments.

45

46 **SIGNIFICANCE STATEMENT**

47 Mitochondria are pivotal for plant metabolism. One of their central functions is to provide carbon
48 intermediates for the synthesis of critical building blocks, such as amino acids. Malate import and
49 citrate export are two of the most recognised and specialised features of the mitochondrial role in the
50 plant cellular metabolic network, yet the possibility that a single carrier would unite both functions has
51 not been considered. Here, we have demonstrated that DIC2 preferentially fulfils these two functions
52 in *Arabidopsis thaliana in vivo*, making it a bifunctional gateway for two major metabolite fluxes into
53 and out of the mitochondrial matrix in the plant cell. Our results highlight the significance of DIC2 in
54 cooperation with other mitochondrial carriers in maintaining metabolic balance even under
55 challenging environmental conditions.

56

57 INTRODUCTION

58 Malate is a prominent metabolite that occupies a pivotal node in the regulation of plant carbon
59 metabolism. It is the mainstay of leaf respiration and metabolic redox shuttling between organelles
60 (1). Early studies with isolated plant mitochondria demonstrated that exogenous malate can be
61 translocated by an unknown mechanism into the mitochondrial matrix where it is then rapidly oxidized
62 by both mitochondrial malate dehydrogenase (mMDH) and malic enzyme (NAD-ME), generating
63 oxaloacetate (OAA) and pyruvate as products (2, 3). OAA inhibits mitochondrial respiration by direct
64 inhibition of succinate dehydrogenase and due to the fact that the chemical equilibrium of the mMDH
65 reaction highly favours OAA conversion to malate, thereby diverting NADH away from the electron
66 transport chain (ETC) (4, 5). The NAD-ME activity prevents OAA accumulation in mitochondria, and
67 thus allows the continued oxidation of malate produced in concert with phosphoenolpyruvate
68 carboxylase and malate dehydrogenase activities in the cytosol (6-8), even in the absence of
69 glycolysis-derived pyruvate. Both experimental evidence and flux-balance model predictions indicate
70 that TCA cycle-driven respiration is largely inhibited in the light and that mMDH generally operates in
71 the reverse direction to facilitate redox coupling, resulting in net mitochondrial OAA import and malate
72 efflux (9-13). At night, the requirement for exchanging reducing equivalents between mitochondria
73 and chloroplasts via a malate valve (1, 14, 15) is believed to be minimal due the cessation of both
74 photorespiration and photoinhibitory conditions. The mitochondrial NAD-ME activity and its transcript
75 abundance is highest in the dark (16), therefore the synthesis and oxidation of malate is expected to
76 be carried out by both mMDH and NAD-ME to support the synthesis of ATP (17). These metabolic
77 conditions would enable maximal citrate oxidation in the mitochondrial matrix (18, 19), with excess
78 citrate being exported for storage in the vacuole (20). Inhibition in the synthesis of citrate from malate-
79 derived OAA in mitochondria and its export leads to floral sterility in potato plants (21) and a change
80 in nitrogen incorporation into amino acids and metabolism in tomato leaves (22). Defects in controlling
81 mitochondrial malate use cause different phenotypic changes and metabolic remodelling: the
82 absence of mMDH activity in *Arabidopsis* results in a slow growth phenotype and an elevated leaf
83 respiration rate (23), and the loss of NAD-ME in *Arabidopsis* causes a significant diversion of excess
84 malate to amino acid synthesis at night (16). Even though the mitochondrial transport of malate and
85 citrate is clearly at the heart of the remarkable metabolic flexibility of plants, the identity of the
86 transporter(s) that underpin those fluxes *in vivo* has remained inconclusive.

87 By identifying homologues of yeast and mammalian carriers in *Arabidopsis thaliana*, several possible
88 candidates that may contribute to mitochondrial malate transport in plants were identified (24-26). In
89 contrast to the historical, well-established models that mitochondrial metabolite transporters are
90 discrete and highly specific (27-29), these carriers appeared to lack substrate specificities under *in*
91 *vitro* conditions – for example, dicarboxylate carrier (DIC) isoforms in proteoliposomes can rapidly
92 exchange sulfate with phosphate, malate, OAA and succinate, with an apparent low exchange activity

93 in the presence of citrate, 2-oxoglutarate and fumarate (24). Although *in vitro* studies have been
94 instrumental to reveal what transport activities can be mediated by a protein, they have limitations
95 that turn out to be critical in the case of plant mitochondrial organic acid transporters. For instance,
96 they cannot suitably consider the – often unknown and probably highly changeable – relative
97 metabolite pool sizes and fluxes that the transporters face *in vivo*. Reconstitution with a specific
98 orientation of the transporter is not possible in most *in vitro* systems, but critical for substrate specificity
99 and respiratory physiology *in vivo*. Further, the specific local lipid environment and the pronounced
100 electrochemical gradients ($\Delta\psi$, ΔpH), both of which are likely to be central for inner mitochondrial
101 membrane transport activity and specificity (17), can only be roughly considered. As such, additional
102 information is needed on the function of any transporter candidate within a physiologically more
103 meaningful context. Yet, *in planta* studies of mitochondrial metabolite transporter function that
104 address the question of their *in vivo* function, requiring a systems perspective to consider their
105 integration in the metabolic network, have been lacking.

106 In this study, we reveal a primary role for DIC2 in malate import and citrate export from Arabidopsis
107 mitochondria. Through a reverse genetic approach in combination with comprehensive *in vitro*, *in*
108 *organello*, and *in vivo* analyses, we obtained strong evidence that plant mitochondrial malate and
109 citrate exchange as mediated by DIC2 plays a critical role in dynamically coordinating anaplerotic
110 metabolism with assimilatory and catabolic pathways between the mitochondria and other cellular
111 compartments.

112

113 RESULTS

114 **DIC2 mutation causes decelerated vegetative growth rate that cannot be compensated by** 115 **other mitochondrial dicarboxylate carrier isoforms**

116 DIC2 is targeted to the mitochondrion when transiently expressed (30) and has recently been
117 identified in the mitochondrial proteome by mass spectrometry (31, 32). When DIC2-GFP is stably
118 expressed in Arabidopsis, the fusion protein was found as spherical to elongated structures that
119 colocalised with the mitochondrial dye tetramethylrhodamine (TMRM) (Fig. S1). No overlapping of
120 signal between DIC2-GFP and chloroplast auto-fluorescence was observed in leaf tissue, indicating
121 that DIC2 localises to mitochondria in Arabidopsis.

122 Three T-DNA insertion lines were obtained in order to study the possible physiological and metabolic
123 consequences of a defect in DIC2 (At4g24570) function *in planta*. Only the homozygous *dic2-1* line
124 has a T-DNA insertion within the open reading frame of *DIC2*, resulting in the complete loss of *DIC2*
125 transcript (Fig. 1A and Fig. S2A). Using selective reaction monitoring mass spectrometry (SRM-MS)
126 to determine protein abundances (33), we found that two different DIC2 peptides, detectable in Col-
127 0, were not detectable above baseline chemical noise in mitochondria isolated from *dic2-1* plants (Fig.

128 1A and Fig. S2B), confirming *dic2-1* as a null mutant for DIC2. Given that *DIC2* is more expressed in
129 green tissues than in roots (24), it is expected that the loss of DIC2 would have a greater impact on
130 vegetative growth. Indeed, the homozygous *dic2-1* was characterized by a significantly decreased
131 rate of rosette expansion (Fig. 1B and Fig. S2C). From day 42, the number of leaves emerged from
132 Col-0 and *dic2-1* was identical, but the mutant leaves were smaller and curly with a more rugose
133 surface (Fig. S2D). *dic2-1* could not reach the full rosette diameter of Col-0 after one week of bolting
134 (Fig. S2E). *dic2-1*-specific phenotypes could be observed regardless of the photoperiod (Fig. S2F).
135 These phenotypes could be restored by introducing *DIC2* under the control of its native promoter
136 (*dic2-1/gDIC2*) or a cauliflower mosaic virus 35S promoter (*dic2-1/DIC2 OE*). While full
137 complementation was reached through the native promoter, 35S-driven expression of *DIC2* resulted
138 in a slight delay in phenotype restoration in the *dic2-1* background and led to a reduced rosette size
139 in Col-0 background (Fig. 1B, Fig. S2G and Table S1), indicating that the correct dose of *DIC2*
140 expression is essential for normal leaf growth.

141 *DIC2* shares high amino acid sequence similarity as well as broad and identical substrate preferences
142 with two mitochondrial dicarboxylate carriers *DIC1* and *DIC3* as determined *in vitro* (24). Liposome-
143 based transport studies also found overlapping substrate preferences with succinate-fumarate carrier
144 1 (SFC1), dicarboxylate-tricarboxylate carrier (DTC) and uncoupling protein 1 (UCP1) (25, 26, 34).
145 The loss of *DIC2* resulted in a modest two- to three-fold increase in *DIC1* and *DIC3* transcripts at
146 night, but not at mid-day, while the transcripts of the other three proteins were not affected (Fig. S2H).
147 To test the hypothesis of functional redundancy within the DIC family, we attempted to rescue the
148 *dic2-1* phenotype by expressing *DIC1* and *DIC3* in the *dic2-1* background (*dic2-1/DIC1 OE* and *dic2-1*-
149 *1/DIC3 OE* respectively), but neither could complement the loss of *DIC2*, not even partially (Fig. 1B).
150 These results indicate that *DIC2* is unlikely to share substrate preferences and/or specificities with
151 *DIC1* or *DIC3* *in planta* and emphasize the need for an *in vivo* assessment.

152 **Malate is the major dicarboxylate substrate of *DIC2* in isolated *Arabidopsis* mitochondria**

153 The inability of *DIC1* or *DIC3* to rescue *dic2-1* phenotypes prompted us to reinvestigate *DIC2* function
154 in detail. In order to maintain *DIC2* close to its true functional context, while being able to control
155 substrate availabilities, we used isolated mitochondria as a model system to connect previous *in vitro*
156 insights from liposome assays and the more complex *in vivo* situation. We first examined if malate
157 and succinate are the main substrates for *DIC2* in isolated mitochondria, as inferred previously by a
158 liposome-based approach (24). To this end, mitochondria purified from Col-0, *dic2-1* and *dic2-1*-
159 *1/gDIC2* were tested for their ability to consume dicarboxylates under state III respiration conditions
160 (measured as O₂ consumption coupled to ATP synthesis) and to generate and export metabolites
161 synthesised from the substrates provided (measured by LC-SRM-MS analysis of the separated
162 mitochondrial and the extra-mitochondrial space fractions; Fig. 2A).

163 Titrations with respiratory substrates at different concentrations revealed no obvious differences in
164 the rate of internal or external NADH-driven O₂ consumption between Col-0 and *dic2-1* (Fig. 2B; Fig.
165 S3A). No change in the abundance or activity of electron transport chain (ETC) supercomplexes (Fig.
166 S4A), the relative abundance of TCA cycle enzymes, pyruvate dehydrogenase or NAD-ME (Fig. S4B),
167 or their K_m and V_{max} (Table S2) were observed when mitochondria isolated from these genotypes
168 were compared. This eliminated the possibility of a clear defect in the ETC or a specific step of the
169 TCA cycle in *dic2-1*; instead, any shift in the distribution of specific metabolites between the matrix
170 and extra-mitochondrial space in the mutant could reasonably be attributed directly to the absence of
171 DIC2 and/or indirectly to the enzymatic regulatory compensation as the result of DIC2 loss.

172 Through the action of the TCA cycle and NAD-ME, imported substrates can generate both OAA and
173 pyruvate (Fig. 2A). Note that it is difficult to experimentally assess OAA and pyruvate independently
174 because OAA undergoes spontaneous decarboxylation into pyruvate; therefore, we considered the
175 pyruvate signal to represent both pyruvate and OAA levels. Upon feeding externally with 500 μM
176 malate, pyruvate and/or OAA abundance increased linearly over time in mitochondria of Col-0 and
177 *dic2-1/gDIC2*, whereas it levelled off in *dic2-1* (Fig. 2C, panel iv). The magnitude of *dic2-1*-specific
178 increase in pyruvate and/or OAA content in mitochondria was far less drastic for succinate or 2-OG
179 feeding, both of which led to the formation of malate within the matrix (Fig. 2C, panel v-vi). Consistent
180 with this, *dic2-1* mitochondria exhibited a 20–30% lower V_{max} for malate-dependent state III O₂
181 consumption at pH 7.2, although the K_m was unchanged (Fig. 2B). When malate-dependent O₂
182 consumption by isolated mitochondria was measured at the optimal pH for NAD-ME activity
183 (pH~6.5)(35), no difference in K_m and V_{max} between *dic2-1* and Col-0 was observed. These data
184 pinpoint reduced malate availability in the matrix of malate-fed *dic2-1* mitochondria as a plausible
185 cause for the observed decrease in malate-dependent respiration (via mMDH) and pyruvate and/or
186 OAA formation. To test more directly whether DIC2 indeed imports malate into mitochondria and
187 whether this import is restricted in *dic2-1*, we monitored the transport activity for ¹⁴C-malate by isolated
188 mitochondria in a reaction medium that lacked cofactors and ADP to allow malate to accumulate while
189 preventing its conversion into other TCA cycle intermediates. Under such conditions, the initial uptake
190 rate of 200 μM [¹⁴C]-malate into mitochondria of *dic2-1* was three-fold lower compared to Col-0 and
191 *dic2-1/gDIC2* (Fig. 2D). Hence, DIC2 possesses a significant malate uptake capacity in isolated
192 Arabidopsis mitochondria even in the presence of other potential carriers for malate transport.

193 If the role of DIC2 in 2-OG and/or succinate uptake is as important as malate transport, mutant
194 mitochondria would be expected to display a lower O₂ consumption rate in their presence as well as
195 to accumulate and/or export less of their nearest TCA cycle product(s) when these substrates are
196 supplied. There was no significant change in succinate-stimulated Complex II-linked O₂ consumption
197 (Fig. 2B), so the mutant growth phenotype was unlikely to be caused by a reduced mitochondrial
198 succinate uptake and oxidation. 2-OG-dependent state III respiration in *dic2-1* mitochondria was

199 reduced in *dic2-1* mitochondria, to an extent which was strikingly similar to malate oxidation at pH 7.2
200 (Fig. 2B). However, DIC2 is unlikely to be a major 2-OG importer, since 2-OG, malate and succinate
201 levels in *dic2-1* mitochondria and extramitochondrial space were not altered when 2-OG was supplied
202 (Fig. S5C). This anomaly between O₂ consumption and substrate accumulation patterns may be
203 explained by a partial feedback inhibition of mMDH reducing NADH necessary for the ETC activities
204 and resulting in a flux diversion of malate to fumarate (Fig. 2A). Consistent with this we observed
205 increases in fumarate accumulation and efflux by *dic2-1* mitochondria when supplied with malate and
206 succinate (Fig. 2E, panel i-ii and iv-v). In addition, it could be due to the observed increase in pyruvate
207 and/or OAA export rate to relief the product inhibition of mMDH when supplied with 2-OG (Fig. 2C,
208 panel ii).

209 **DIC2 is one of the mitochondrial carriers that determine the fate of citrate in energised** 210 **mitochondria**

211 The other main discovery from our substrate feeding experiments was a much higher amount of citrate
212 accumulating inside *dic2-1* than Col-0 mitochondria after malate (Fig. 2F panel iii), succinate or 2-OG
213 feedings (Fig. S5C-D). If OAA and/or pyruvate exports were also limited in *dic2-1* mitochondria, matrix
214 pyruvate and/or OAA contents would be expected to accumulate more over time with a slower
215 combined rate of their export to the extramitochondrial space. However, pyruvate and/or OAA appear
216 to be maintained in the mutant mitochondria in the same way as in Col-0 after malate or succinate
217 feedings (Fig. 2C, panel i and iii). In contrast, the rate of export of citrate to the extra-mitochondrial
218 space was decreased in *dic2-1* mitochondria when compared to Col-0 and *dic2-1/gDIC2* in malate
219 (Fig. 2F panel i), succinate or 2-OG feedings (Fig. S5C-D). The degree of decrease in each case was
220 different depending on substrate concentration and the number of subsequent enzymatic steps
221 leading to citrate formation. We hypothesised that excess citrate in *dic2-1* mitochondria was caused
222 by a defect in citrate export which then prevented OAA condensation in the citrate synthase reaction
223 and thus suppressed mMDH activity (36). To confirm this, we tested the ability of mitochondria to
224 directly consume citrate (Fig. S5E). Under such conditions, NAD-ME and mMDH activities became
225 inhibited, as demonstrated by the low mitochondrial export rate of pyruvate and/or OAA (Fig. S5E).
226 There was no change in citrate-dependent O₂ consumption mitochondria from all genotypes (Fig. 2B),
227 further confirming that citrate import was not affected and the reduction in malate- and 2-OG-
228 dependent respiration by *dic2-1* was likely caused by the citrate accumulation in the matrix triggering
229 an OAA inhibition of mMDH.

230 While the uptake rates of citrate by mitochondria were not altered significantly over time (Fig. 2F,
231 panel ii), the rate of citrate accumulation in *dic2-1* mitochondria was two- to three-fold higher than Col-
232 0 or *dic2-1/gDIC2* (Fig. 2F, panel iv). *dic2-1* mitochondria appeared to be oxidising excess citrate
233 through the TCA cycle (Fig. 2A) as evident by a higher rate of 2-OG and fumarate accumulation in
234 *dic2-1* mitochondria and an increased fumarate export (Fig. 2E, panel iii and vi; Fig. S5E). Similar

235 results were also observed when mitochondria were externally provided with isocitrate (Fig. S5F). We
236 could not observe any obvious change in import and export rates of succinate, 2-OG and pyruvate by
237 *dic2-1* mitochondria, indicating that other carriers with a similar set of *in vitro* substrates as DIC2, as
238 previously observed in proteoliposome-based studies, may be able to compensate for its absence.
239 Taken together, DIC2 is directly responsible for malate uptake, and we hypothesised that either citrate
240 is the counter ion, or DIC2 is able to separately transport these organic acids in opposing directions.
241 The fact that citrate export was not completely abolished by the loss of DIC2 would suggest that there
242 are also other citrate export carriers present in the inner mitochondrial membrane.

243 **DIC2 function effects leaf dark respiration by modulating NAD homeostasis**

244 We then set out to determine if defects in mitochondrial malate import and citrate export operate *in*
245 *planta* and if they could explain the observed phenotypes of *dic2-1*. In total we investigated three
246 scenarios where leaf mitochondria operate under different flux modes: in the light, during the transition
247 from light to dark and in the dark. We first carried out chlorophyll fluorescence and infrared gas-
248 exchange analyses at different light intensities, because changes in photosynthetic performance can
249 cause many metabolic perturbations and mask other primary metabolic effects in mutants. There was
250 no change in the CO₂ assimilation rate (Fig. 3A), stomatal conductance, transpiration rate,
251 photosynthetic electron transport rate, photosystem II quantum yield or nonphotochemical quenching
252 in *dic2-1* leaves (Fig. S6A-E). When plants were shifted to high light for 3- and 16-h, we did not detect
253 any changes in the maximum photochemical efficiency of PSII (F_v/F_m) between *dic2-1*, Col-0 and *dic2-*
254 *1/gDIC2* (Fig. S6F). These results indicated that the loss of DIC2 has no direct impact on
255 photosynthetic performance.

256 We next examined the transition from light to darkness where leaf mitochondria undergo several rapid
257 changes in metabolic activity as photorespiration ceases and non-cyclic mode of the mitochondrial
258 TCA cycle is activated. Upon transfer of illuminated leaves to darkness, *dic2-1* exhibited a more rapid
259 release of CO₂ in the first 30-40 s before reaching a higher rate of steady-state respiratory CO₂ release
260 compared to Col-0 and *dic2-1/gDIC2* (Fig. 3B). The sharp CO₂ release upon sudden darkness is
261 indicative of a post-illumination burst (PIB) of respiration, an estimate of the degree of respiratory
262 glycine oxidation (37). To examine if photorespiratory activities were altered in the mutant, we grew
263 the mutant under high CO₂ (0.2%) to suppress photorespiration but no rescue of the phenotype was
264 achieved (Fig. S6G). These data indicate that an altered photorespiratory activity after dark shift is
265 not the primary cause for the change in PIB response by *dic2-1*. Since malate/OAA utilisation in
266 mitochondria can control the degree of glycine oxidation by regulating NADH/NAD⁺ levels (e.g. via a
267 malate shuttle) (4), we hypothesised that a PIB increase in *dic2-1* could be linked to altered distribution
268 of TCA cycle metabolites between mitochondria and cytosol (and possibly plastids), leading to
269 changes in metabolic and/or NAD redox state in these compartments. To capture any rapid and
270 transient changes in NAD redox state during a sudden dark shift, we utilised a fluorescent protein

271 biosensor Peredox-mCherry which reports cytosolic NADH/NAD⁺ through the ratio of tSapphire to
272 mCherry fluorescence ($\log_{10}(tS/mC)$), where a higher $\log_{10}(tS/mC)$ corresponds to a more reduced
273 NAD pool (38, 39). We observed equally high NADH/NAD⁺ ratios in Col-0 and *dic2-1* plants during
274 illumination (Fig. 3C). However, upon transfer to darkness, the expected decline in NADH/NAD⁺ ratios
275 in the first 100 seconds was significantly slower in *dic2-1* compared to Col-0. Both differences in PIB
276 and NAD redox status upon rapid transition to darkness indicate some defect in switching between
277 light and dark flux modes by *dic2-1* mitochondria.

278 Thirdly, we examined metabolic changes to *dic2-1* leaves during the night. DIC2 expression steadily
279 increased over the course of night-time, followed by a decline from the peak at the end of dark
280 photoperiod to the lowest level in the light (Fig. S6H). Intriguingly, while there was no difference in the
281 NADH/NAD⁺ ratio between the two genotypes over the course of the dark-light-cycle (Fig. 3D), the
282 leaf night time respiration rate (R_N) remained consistently higher in the mutant (Fig. 3E). Given that
283 primary metabolites are crucial determinants for regulating transcript abundance during a diurnal
284 cycle (40), there appears to be a metabolic rearrangement in the mutant to avoid any detrimental
285 impact of DIC2 absence on NAD redox equilibrium, albeit at the expense of heightened respiration
286 (Fig. 3B and 3E) and slower vegetative growth (Fig. 1B). Taken together, DIC2 activity may have a
287 greater influence on metabolism and mitochondrial respiration in the dark, most likely through
288 modulating the TCA cycle steps in the cytosol and/or mitochondria to maintain metabolic homeostasis
289 required for fundamental cellular functions.

290 **2-oxoglutarate sharply accumulates in *dic2-1* leaves upon shift to darkness**

291 To gain further insight into how DIC2 transport functions are integrated into metabolism and influences
292 NAD redox state *in vivo*, we carried out metabolite profiling of 6-week-old leaf samples collected at
293 different time points of a diurnal cycle (Fig. 4A and Fig. S7). The metabolite profiles of malate,
294 fumarate and succinate over a diurnal cycle were generally similar between genotypes. Also, a similar
295 pattern in daytime glycine and serine accumulation was observed, despite a clear difference in PIB
296 (Fig. 3B), further confirming that DIC2 function does not directly affect photorespiratory flux. The most
297 notable metabolite level changes in *dic2-1* plants compared to Col-0 and *dic2-1/gDIC2* were observed
298 in the first-hour after the sudden shift to darkness, including two- to four-fold higher abundances of
299 pyruvate, citrate and isocitrate, and a remarkable 10-fold increase in 2-oxoglutarate abundance (2-
300 OG). Several amino acids linked to 2-OG utilization also changed in abundance in *dic2-1*. In particular,
301 the glutamate pool in *dic2-1* was larger than Col-0 and *dic2-1/gDIC2* plants one hour after the dark
302 shift and during the light photoperiod, while GABA and glutamine abundances remained unchanged.
303 Aspartate and alanine, which can be converted into OAA and pyruvate respectively in a reversible
304 reaction that requires glutamate/2-OG transamination, were also more abundant in *dic2-1* after one
305 hour of darkness, while aspartate-derived threonine accumulated in the mutant throughout the diurnal
306 cycle. Branched chain amino acids (BCAAs), which use 2-OG as co-substrate to initiate their

307 catabolism in mitochondria (41), were generally higher in abundances in *dic2-1* plants at night.
308 Overall, the metabolite profiles revealed that the loss of DIC2 function causes an impaired 2-OG
309 metabolism in the dark, which may provide a metabolite buffer to compensate for a defect in
310 mitochondrial DIC2 transport activity while cytosolic NAD redox state is maintained.

311 **A defect in organic acid use causes accelerated leaf senescence of the DIC2 knockout during** 312 **prolonged darkness**

313 Elevated level of BCAAs in *dic2-1* (Fig. 4A) may indicate a possible defect in mitochondrial BCAA
314 catabolism due to changes in the uptake of BCAAs and/or their derivatives into the matrix. Most BCAA
315 catabolism mutants accumulate BCAAs and are more susceptible to early senescence during
316 prolonged darkness (42-47). To test if intermediates of BCAA catabolism could also be DIC2
317 substrates, we subjected Arabidopsis plants to darkness for 15 days. The mutant exhibited an
318 accelerated decline in F_v/F_m beginning around 7 days of darkness (Fig. S8A). Leaves of *dic2-1* were
319 more yellowed compared with the Col-0 and the *dic2-1/gDIC2* after 12 days (Fig. S8B). When 15 days
320 dark-treated plants were transferred back to the normal short-day cycle, only Col-0 and *dic2-1/gDIC2*
321 could recover after seven days. Next, we measured the abundance of organic acids, amino acids and
322 branched chain 2-oxoacids (BCKA) in 10 days dark-treated transgenic plants with known
323 mitochondrial responses to carbon starvation (Fig. 4B). Knockout mutants with defects in
324 mitochondrial BCAA catabolism, *mcca1-1*, *mccb1-1* and *hml1-2*, displayed accelerated senescence
325 and had higher amounts of BCAAs than Col-0 as observed previously (43, 48), as well as
326 accumulated BCKA. In comparison, the double knockout of glutamate dehydrogenase (*gdh dKO*),
327 which does not directly participate in BCAA catabolism but senesces more rapidly under prolonged
328 darkness (49), significantly accumulated BCAAs without altering the abundance of BCKA. The loss
329 of DIC2 resulted in slight but significant accumulation of valine but not leucine, isoleucine and BCKAs
330 when compared to Col-0 and two different complemented lines. These results indicate that DIC2 is
331 not involved directly in the transport of BCAAs or their derivatives.

332 Strikingly, all TCA cycle intermediates were significantly higher in abundance in *dic2-1* upon 10 days
333 of dark treatment, whereas other mutants only displayed minor changes. To identify the TCA cycle
334 metabolites that were affected the most by the absence of DIC2, we carried out a time-course
335 measurement of organic acids contents over 12 days of prolonged darkness (Fig. 4C and Fig. S8C).
336 When F_v/F_m began to decline more rapidly in *dic2-1* on day 7 (Fig. S8A), only malate, 2-OG and citrate
337 were significantly more accumulated. While all TCA cycle intermediates were significantly increased
338 in the mutant 10 days after dark treatment, malate and 2-OG accumulated at least 10 times higher in
339 abundance in the mutant than Col-0 and *dic2-1/gDIC2*. Citrate abundance in the Col-0 and *dic2-1/gDIC2*
340 progressively declined from day 3 to day 12 of darkness, whereas it remained unchanged in
341 *dic2-1* plants throughout the treatment. Notably, the accumulation of these metabolites by *dic2-1* in
342 *planta* would be consistent with a failure to properly regulate mitochondrial malate import and citrate

343 export. Throughout a diurnal cycle, pool sizes of these metabolites were unchanged (Fig. 4A); it was
344 only when plants were exposed to dark-induced starvation that altered patterns in the utilization of
345 specific organic acids manifested (Fig. 4C).

346 **DIC2 modulates metabolic flux through TCA cycle and amino acid metabolism to support** 347 **citrate export at night**

348 We next further investigated the cause of the increased R_N in *dic2-1*. An increased night-time
349 consumption rate of sucrose, but not of glucose or fructose, by *dic2-1* was observed (Fig. 5A and Fig.
350 S9A). The expression of several nutrient-responsive senescence markers, SAG101 (50), WRKY53
351 (51) and SEN1 (52), were also highly upregulated in the mutant in the dark but not in the light (Fig.
352 5B and Fig. S9B), suggesting night time starvation. These results, combined with a lack of
353 photosynthetic differences (Fig. 3A, Fig. S6A-E), suggest that an accelerated depletion rate of carbon
354 stores via respiration is leading to night time starvation in *dic2-1*. Thus, changes in metabolite
355 abundances noted above were accompanied by a higher sucrose catabolism in the mutant at night.
356 When leaf discs were incubated in the dark with uniformly labelled ^{14}C -malate or ^{14}C -leucine and the
357 evolution of $^{14}\text{CO}_2$ was monitored, we found that *dic2-1* showed higher $^{14}\text{CO}_2$ emissions than Col-0
358 and *dic2-1/gDIC2* from malate but not leucine (Fig. 5C). The observed increase in BCAAs
359 accumulation in *dic2-1* in the dark (Fig. 4A) was contributed by increased TCA cycle fluxes into
360 biosynthetic pathways and/or an elevated proteolysis, while BCAAs breakdown for respiration
361 remained unchanged. Thus, these data indicated that the loss of DIC2 results in increased sucrose
362 utilization (or export for use by other tissues) and TCA cycle-facilitated respiration to compensate for
363 a failure to maintain the homeostasis of organic acid oxidation.

364 The observed decrease in substrate-dependent O_2 consumption by isolated mitochondria (Fig. 2B)
365 did not explain the faster dark respiration of intact leaves (Fig. 3E). This could be due to the absence
366 of any extramitochondrial metabolism, which *in vivo* maintains metabolite supply for sustaining
367 mitochondrial transport activities, TCA cycle and respiration in response to rearranged metabolism
368 and transport in the mutant. To account for the apparent homeostasis in metabolite pool sizes (Fig.
369 4A), we postulated that there could be a flux change in certain steps of metabolism to compensate
370 for the reduced malate import and citrate export from mitochondria. To determine if *dic2-1* metabolises
371 carbon differently, we traced the flux of U- ^{13}C -glucose into the TCA cycle and closely related amino
372 acids in leaf discs in the dark for 8 hours, and the ^{13}C -tracing data was normalised by taking into
373 consideration the differences in dark respiration rate (Fig. 5D; SI Dataset 1; SI Methods). Consistent
374 with DIC2's proposed function as a citrate transporter, *dic2-1* displayed a decreased rate of citrate
375 labelling over the course of dark incubation (Fig. 5E). Such a decrease was unlikely to be contributed
376 by a reduction in peroxisomal citrate synthase because labelled acetyl-CoA cannot be directly
377 exported from mitochondria (53), and the existence of a carnitine/acylcarnitine carrier in plant
378 mitochondria is questionable since its closest homolog BOU has recently been reported to transport

379 glutamate (54). On the other hand, the citrate pool remained stable in the dark in *dic2-1* (Fig. 4A)
380 possibly due to compensation by altered citrate turnover rates in other compartments. A decrease in
381 OAA availability from cytosolic phosphoenolpyruvate (PEP) carboxylase could also be ruled out, since
382 labelling of m+3 aspartate (a proxy for labelled OAA) was not altered (Fig. S10A). Decreased citrate
383 labelling was accompanied by a significant increase in the abundance of labelled 2-OG due to a higher
384 total pool in the mutant (Fig. 5F; SI Dataset 1), which coincided with an increased rate of ¹³C
385 incorporation into glutamine (Fig. 5G). These increases could be facilitated by a higher mitochondrial
386 glutamate efflux rate since there was a higher 2-OG accumulation in citrate-fed *dic2-1* mitochondria
387 (Fig. S5E), implying that an enhanced flux into glutamine was necessary to remove excess
388 mitochondrial 2-OG by mitochondrial glutamate transamination reactions in concert with plastidic
389 glutamine synthase (55). Downstream extra-mitochondrial biosynthetic pathway of aspartate-derived
390 amino acids, asparagine and threonine, were increased in abundances in the mutant (Fig. 5H-I), while
391 the amount of labelled succinate, fumarate, malate and aspartate via the TCA cycle or PEP-OAA
392 interconversion did not change (Fig. 5J and Fig. S10B-D). All these increases are consistent with a
393 metabolic diversion of excess malate that was not consumed by mitochondria for citrate synthesis
394 (due to a decrease in malate uptake and product inhibition of mMDH in the matrix) into aspartate.
395 Overall, the ¹³C feeding data helped to explain how the mitochondrial phenotypes of *dic2-1* loss (Fig.
396 2) are significantly overcome in a whole plant metabolic context to establish day and night
397 homeostasis and retain a viable plant albeit with stunted growth rate (Fig. 1). Only at day to night
398 transitions and prolonged darkness do the consequences of these unusual metabolic fluxes yield
399 temporary gross imbalances in metabolite pools.

400 DISCUSSION

401 It was reported that DIC2, DIC1 and DIC3 are carriers for malate and OAA exchange to regulate NAD
402 redox and photorespiration in the light (56-58). In addition, several mitochondrial malate carriers,
403 including DIC2, were found to have a broad substrate preference for other dicarboxylates,
404 tricarboxylates and/or amino acids with close resemblance to dicarboxylates *in vitro* (24-26), but their
405 actual contributions to mitochondrial malate transport *in organello* or *in planta* have not been verified.
406 Determining if these types of carriers are generalists or specialists *in vivo* is critical in any future
407 attempt to modify mitochondrial substrate use, or to understand if transport is a point of control in
408 metabolic models of plant cell function.

409 Malate import and citrate export are two of the most critical fluxes that mitochondria contribute to the
410 rest of the cellular metabolic network in plants (59-61). Malate plays a pivotal role in mediating
411 metabolic redox exchange between cellular compartments (57, 62). On the one hand, citrate
412 produced in mitochondria is the major source of cellular citrate when the TCA cycle operates at night
413 in mature green leaves. Here, we identified DIC2 as a single carrier linking these functions to
414 mitochondrial anaplerotic metabolism. While our data reveal that other carriers can also mediate at

415 least one of these two functions to provide partial functional backup, that is, however, insufficient to
416 maintain metabolism unperturbed.

417 Given the prior evidence of broad DIC1 substrate preference *in vitro* and high amino acid identity
418 among the DIC homologs, our finding that DIC1 could not complement the *dic2-1* phenotype (Fig. 1B,
419 Fig. S2H) was unexpected (Fig. S11). Yet, inferring *in vivo* function from *in vitro* data on transport
420 specificity data is known to be problematic and has prevented capture of the biological importance of
421 transport of other substrates. For example, PAPST1 and PAPST2, which are 78% identical in amino
422 acid sequence, both transport 3'-phosphoadenosine 5'-phosphate (PAP) and 3'-phosphoadenosine
423 5'-phosphosulfate (PAPS) in liposomes with only slight differences in their efficiency in driving ATP
424 exchange (63). However, their true *in vivo* function was revealed only after additional genetic,
425 biochemical and metabolomic approaches were employed: PAPST1 being responsible for the
426 majority of PAPS/PAP transport to regulate glucosinolate biosynthesis in plastids, while PAPST2
427 fulfils a stress signalling role through PAP/AT(D)P exchange in chloroplasts and mitochondria (63,
428 64). In a similar way, while liposomes showed the ability of DIC2 to transport a variety of
429 dicarboxylates and even citrate, albeit poorly (24), they could not accurately predict apparent
430 specificity or directionality of transport in intact mitochondria (Fig. 2) or the *in vivo* consequences of
431 DIC2 loss (Fig. 3-5).

432 Revealing the role for DIC2 in citrate export required moving to a less reductionist system, i.e. to the
433 exploration of metabolic processes in isolated mitochondria (Fig. 2). Citrate produced in the
434 mitochondria is predicted to be exported for fatty acid biosynthesis via the cytosolic ATP-dependent
435 citrate lyase (65), or for storage in the vacuole based on flux prediction and ¹³C labelling analysis (20,
436 66), although it is also possible to fuel respiration in mitochondria isolated from storage tissues by
437 externally supplying an excess amount of citrate (67). Given the importance of mitochondria-supplied
438 citrate to metabolism in green tissues, it is expected that a complete block in mitochondrial citrate
439 synthesis and export would result in severe reduction in post-germination vegetative growth. A null
440 mutant of mitochondrial citrate synthase has not been reported to date, and a reduction in
441 mitochondrial citrate synthase activity only resulted in a small change in vegetative growth phenotype
442 (21, 22). Unlike in yeast and mammals, the function of plant mitochondrial pyruvate carrier (MPC)
443 seems to be non-essential since its absence has no effect on growth or the cellular citrate pool (16,
444 68). In comparison, mutants lacking the activity in one of the subunits of mitochondrial pyruvate
445 dehydrogenase complex (mPDC) or both mMDH isoforms, which catalyse acetyl-CoA and OAA
446 formation respectively required for citrate synthesis, are significantly slower in vegetative growth (23,
447 69, 70). mPDC mutation causes a severe blockage in citrate generation in leaf (69) that does not
448 appear to be compensated by altering pyruvate decarboxylation and citrate synthesis activities in
449 other compartments. By contrast, OAA import into the mitochondria is sufficient to maintain a citrate
450 pool in the mMDH double knockout similar to that in the wildtype at the expense of elevated respiration

451 and increased accumulation of dicarboxylates (23). Here, we observed a reduction in vegetative
452 growth in *dic2-1*, with decreases in citrate export by isolated mitochondria (Fig. 2F) and *in vivo* ¹³C-
453 glucose labelling into citrate (Fig. 5E) when compared to the wildtype. Unlike mMDH and mPDC
454 mutants, however, the steady state pool of organic acids, including citrate, was surprisingly stable in
455 *dic2-1* (Fig. 4A). This suggests that fatty acid turnover is affected, either through increasing citrate
456 synthesis via the last step of peroxisomal β -oxidation and/or decreasing citrate breakdown during the
457 initial steps of plastidic fatty acid biosynthesis. The former is a more likely scenario given that *dic2-1*
458 phenotypes are observed mostly during darkness when fatty acid biosynthesis is ineligible (71), and
459 the transcripts of two peroxisomal citrate synthase isoforms are more abundant at night (72, 73) and
460 during prolonged darkness (74). Lowering fatty acid accumulation by limiting triacylglycerol depletion
461 helps plants survive prolonged darkness by dampening the degree of lipid peroxidation (75). Thus,
462 the increased susceptibility to dark-induced senescence by *dic2-1* (Fig. 4B-C and Fig. S8) could be
463 caused by a loss of synchronisation in fatty acid turnover with peroxisomal citrate synthesis and
464 export, as a result of increased demand for peroxisomal citrate to compensate for a reduction in
465 mitochondrial carbon supply. The requirement for an equilibrium between organellar citrate synthesis
466 and fatty acid breakdown to prevent excess reactive oxygen species accumulation would reasonably
467 explain why a strong DIC2 transcriptional response is commonly observed during abiotic stress
468 treatments, including touch and sound vibration (76, 77), phosphate deficiency (78), light-to-dark
469 transition (79) and cold, drought and UV stresses (80). Overall, these data strongly support a function
470 of DIC2 in plant mitochondrial citrate transport, with a reduction in citrate export as a direct
471 consequence of DIC2 loss, rather than a side effect.

472 The existence of multiple modes of TCA cycle substrate transport has been proposed (27, 28) but the
473 lack of clarity as to the identity and substrate specificity of carriers responsible has been hindering
474 our understanding on how they cooperate to support the integration of mitochondrial carbon
475 metabolism into the wider cellular metabolic network (17). In the case of *dic2-1*, we found that there
476 was no change in the uptake of externally supplied substrate by fully energised isolated mitochondria
477 (Fig. S5 "INPUT"). Residual malate import and citrate export are maintained in *dic2-1* mitochondria
478 (Fig. 2F, Fig. S5B), suggesting that other carriers exist to partially compensate for the absence of
479 DIC2 activity. The majority of an added dicarboxylate was oxidised to pyruvate and/or OAA in mutant
480 mitochondria with a diversion of excess malate destined for OAA and citrate formation into a hydration
481 reaction to produce fumarate, which was then exported from isolated mitochondria (Fig. 2E) and
482 redirected towards aspartate metabolism *in vivo* as seen by increases in asparagine and threonine
483 labelling (Fig. 5H-I). It is remarkable that, despite all these changes, *in vivo* cytosolic NADH/NAD⁺
484 ratios in *dic2-1* leaves did not differ from wildtype throughout the night (Fig. 3D) with only a glimpse
485 of change during a light-to-dark transition (Fig. 3C). We speculate that the homeostasis of NAD redox
486 state in the mutant can be explained by at least one of the following: (i) an increased rate of malate

487 oxidation being offset by a reduction in isocitrate oxidation in the cytosol; (ii) a rapid remobilisation of
488 excess NADH into the intermembrane space of mitochondria where it was oxidised by external NADH
489 dehydrogenase, thereby raising leaf respiration in the dark (Fig. 3E); and/or (iii) excess reductant
490 used for diverting malate into threonine generation via aspartate catabolism, requiring 2 NADPH and
491 2 ATP molecules (81). Consistently, metabolite labelling and profiling have highlighted the flexibility
492 of metabolism when multiple carriers with varying substrate preferences are present. For instance,
493 the loss of mitochondrial citrate carrier in *Drosophila* larvae causes only a mild reduction in citrate
494 content concomitant with increased malate and fumarate levels (82). Malate and citrate levels are
495 slightly decreased in mice with suppressed expression of the mitochondrial dicarboxylate carrier (83).
496 Silencing of the mitochondrial glutamate carrier in colorectal tumor cells resulted in a relatively small
497 increase in cellular glutamate content whereas the aspartate level was reduced by ~45% (84). In
498 plants, studies of mitochondrial carrier mutants reported to date are unable to directly link growth
499 and/or metabolic phenotype with gene function (85-87). It is possible that, apart from functional
500 redundancy, changes in metabolic fluxes occur without altering overall metabolite pool or physiology,
501 which can only be captured by sensitive measurements under specific external conditions.

502 In conclusion, we have refined the current molecular identity of DIC2 to be a mitochondrial malate
503 import and citrate export carrier in Arabidopsis, the absence of which leads to growth retardation. The
504 importance of mitochondrial organic acid exchange carriers in plants has been discussed for decades,
505 but it is only in the last decade that their identities are beginning to be unravelled through heterologous
506 systems. By utilising a broad approach in combination with reverse genetics, however, we
507 demonstrate that carrier analysis in heterologous systems are only the start to reveal the true nature
508 of DIC2 *in vivo*. Given the lack of genetic clarity of many plant mitochondrial carriers, it is reasonable
509 to suspect that the true identity of many other carriers has yet to be unravelled. Here, we provide a
510 blueprint for characterising the *in organello* and *in vivo* function of a plant mitochondrial carrier that
511 requires an integrated approach to analyse genetic lines. Such approaches reveal systems
512 characteristics that may be strictly required from carrier function and specificity, such as exact
513 membrane composition, bioenergetic status, pH and relative local metabolite pool sizes and fluxes.
514 A complete, precise identification of mitochondrial metabolite carriers and their substrate preferences
515 with kinetic characteristics and transport orientation will assist in improving genome scale metabolic
516 models, as well as refining the role of DIC2 role in underpinning the remarkable flexibility of plant cell
517 metabolism.

518

519 **METHODS**

520 **Plant Material and Growth Conditions**

521 The *DIC2* T-DNA insertion lines were obtained from GABI-Kat (*dic2-1* GK-217B05, *dic2-2* GK-833F11
522 and *dic2-3* GK-047F03)(88). *gdh* dKO (*gdh1-2 x gdh2-1*), *mcca1-1*, *mccb1-1* and *hml1-2* were
523 obtained from Arabidopsis Biological Resource Center (CS860075, CS66518, CS66519 and
524 CS66521 respectively (49, 89)). A detailed description of growth conditions, generation of transgenic
525 lines and quantitative transcript analysis is provided in SI Methods.

526 **Isolation of mitochondria, O₂ electrode measurements, enzyme activity assays and metabolite** 527 **uptake assays by silicone oil centrifugation**

528 Mitochondria were isolated from two-week-old Arabidopsis seedlings as described previously (90).
529 O₂ consumption by purified mitochondria was measured in a computer-controlled Clark-type O₂
530 electrode unit according to Lee et al. (91). *In vitro* activities of TCA cycle enzymes in isolated
531 mitochondria were measured as described by Huang et al. (92). Time-course measurements of
532 substrate uptake by isolated mitochondria were carried out using silicone oil centrifugation technique
533 according to Lee et al. (93) with modifications. Fractions above (extra-mitochondrial space) and
534 bottom (pellet, mitochondria) were collected, and metabolites were methanol-extracted and detected
535 by mass spectrometry. Additional information is provided in SI Methods.

536 **Analyses of metabolites by mass spectrometry**

537 For GC-MS analysis of sugars, derivatised metabolite samples were analysed by an Agilent 6890 gas
538 chromatograph coupled with a 7683B Automatic Liquid Sampler and a 5973N mass selective
539 detector. For SRM-MS analysis of organic acids. For measuring organic acids amino acids, samples
540 were analysed by an Agilent 1100 HPLC system coupled to an Agilent 6430 Triple Quadrupole (QQQ)
541 mass spectrometer equipped with an electrospray ion source. A detailed description is provided in SI
542 Methods.

543 **¹³C-glucose labelling of Arabidopsis leaf discs and analysis of labelled metabolites**

544 Leaf discs (~50 mg) were prepared from short-day grown (8-h light/16-h dark) plants 1 hour before
545 the end of a normal light photoperiod. They were floated on leaf respiratory buffer containing 20 mM
546 U-¹³C-glucose (99% purity, Sigma Aldrich). At the specified incubation time, leaf discs were briefly
547 washed with respiratory buffer to remove excess labelled glucose and frozen in liquid nitrogen for
548 metabolite extraction as stated above. Analyses of total, untargeted metabolites were performed
549 using an Agilent 1100 HPLC system coupled to an Agilent 6510 Quadrupole/Time-of-Flight (Q-TOF)
550 mass spectrometer equipped with an electrospray ion source. Peak extraction, isotopic correction for
551 natural ¹²C abundances and analysis of isotopic abundances are described in SI Methods.

552 **Relative quantitation of mitochondrial protein abundances by LC-MRM-MS**

553 Multiple reaction monitoring (MRM) was carried out exactly as described previously (94), except
554 trypsin was added to the protein samples in a mass ratio of 1:20. Peptide abundances from each

555 sample were normalised against VDAC in which its abundance was identical between mitochondria
556 from Col-0, *dic2-1* and *dic2-1/gDIC2* based on western blotting. Transitions used for multiple reaction
557 monitoring are provided in Table S3.

558

559 **ACKNOWLEDGEMENT**

560 This work was supported by the Australian Research Council (ARC) Centre of Excellence in Plant
561 Energy Biology (A.H.M., grant number CE140100008) and the German Research Foundation (DFG)
562 (M.S., grant number SCHW1719/5-1 as part of the package grant PAK918). We also thank Dr
563 Brendan O'Leary (The University of Western Australia) for a critical reading of the manuscript.

564 **REFERENCES**

- 565 1. Scheibe R (2004) Malate valves to balance cellular energy supply. *Physiologia Plantarum* 120(1):21-26.
566 2. Coleman JOD & Palmer JM (1972) The oxidation of malate by isolated plant mitochondria. *European Journal*
567 *of Biochemistry* 26(4):499-509.
568 3. Rustin P, Rötig A, & Alin M-F (1985) Continuous measurement of oxaloacetate in purified mitochondria from
569 the leaves of *Kalanchoë blossfeldiana*. *Physiologia Plantarum* 63(2):201-207.
570 4. Journet E-P, Neuburger M, & Douce R (1981) Role of glutamate-oxaloacetate transaminase and malate
571 dehydrogenase in the regeneration of NAD⁺ for glycine oxidation by spinach leaf mitochondria. *Plant*
572 *Physiology* 67(3):467-469.
573 5. Kearney EB, Ackrell BAC, & Mayr M (1972) Tightly bound oxaloacetate and the activation of succinate
574 dehydrogenase. *Biochemical and Biophysical Research Communications* 49(4):1115-1121.
575 6. Day DA & Hanson JB (1977) Pyruvate and malate transport and oxidation in corn mitochondria. *Plant*
576 *Physiology* 59(4):630-635.
577 7. Wiskich JT & Day DA (1982) Malate oxidation, rotenone-resistance, and alternative path activity in plant
578 mitochondria. *Plant Physiology* 70(4):959-964.
579 8. Lance C & Rustin P (1984) The central role of malate in plant metabolism. *Physiologie Végétale* 22:625-641.
580 9. de Oliveira Dal'Molin CG, Quek L-E, Palfreyman RW, Brumbley SM, & Nielsen LK (2010) C4GEM, a
581 genome-scale metabolic model to study C₄ plant metabolism. *Plant Physiology* 154(4):1871-1885.
582 10. Tcherkez G, Cornic G, Bligny R, Gout E, & Ghashghaie J (2005) *In vivo* respiratory metabolism of illuminated
583 leaves. *Plant Physiology* 138(3):1596-1606.
584 11. Tcherkez G, *et al.* (2009) *In folio* respiratory fluxomics revealed by ¹³C isotopic labeling and H/D isotope
585 effects highlight the noncyclic nature of the tricarboxylic acid "cycle" in illuminated leaves. *Plant Physiology*
586 151(2):620-630.
587 12. Hüdig M, *et al.* (2015) Plants possess a cyclic mitochondrial metabolic pathway similar to the mammalian
588 metabolic repair mechanism involving malate dehydrogenase and L-2-hydroxyglutarate dehydrogenase.
589 *Plant and Cell Physiology* 56(9):1820-1830.
590 13. Bykova NV, Møller IM, Gardeström P, & Igamberdiev AU (2014) The function of glycine decarboxylase
591 complex is optimized to maintain high photorespiratory flux via buffering of its reaction products.
592 *Mitochondrion* 19, Part B:357-364.
593 14. Kromer S (1995) Respiration during photosynthesis. *Annual Review of Plant Physiology and Plant Molecular*
594 *Biology* 46(1):45-70.
595 15. Raghavendra AS & Padmasree K (2003) Beneficial interactions of mitochondrial metabolism with
596 photosynthetic carbon assimilation. *Trends in Plant Science* 8(11):546-553.
597 16. Tronconi MA, *et al.* (2008) Arabidopsis NAD-malic enzyme functions as a homodimer and heterodimer and
598 has a major impact on nocturnal metabolism. *Plant Physiology* 146(4):1540-1552.
599 17. Lee CP & Millar AH (2016) The plant mitochondrial transportome: Balancing metabolic demands with
600 energetic constraints. *Trends in Plant Science* 21(8):662-676.
601 18. Igamberdiev AU, Romanowska E, & Gardeström Per (2001) Photorespiratory flux and mitochondrial
602 contribution to energy and redox balance of barley leaf protoplasts in the light and during light-dark
603 transitions. *Journal of Plant Physiology* 158(10):1325-1332.
604 19. Tovar-Méndez A, Miernyk JA, & Randall DD (2003) Regulation of pyruvate dehydrogenase complex activity
605 in plant cells. *European Journal of Biochemistry* 270(6):1043-1049.
606 20. Cheung CYM, Poolman MG, Fell DA, Ratcliffe RG, & Sweetlove LJ (2014) A diel flux balance model captures
607 interactions between light and dark metabolism during day-night cycles in C₃ and Crassulacean acid
608 metabolism leaves. *Plant Physiology* 165(2):917-929.
609 21. Landschütze V, Willmitzer L, & Müller-Röber B (1995) Inhibition of flower formation by antisense repression
610 of mitochondrial citrate synthase in transgenic potato plants leads to a specific disintegration of the ovary
611 tissues of flowers. *The EMBO Journal* 14(4):660-666.
612 22. Sienkiewicz-Porzucek A, *et al.* (2008) Mild reductions in mitochondrial citrate synthase activity result in a
613 compromised nitrate assimilation and reduced leaf pigmentation but have no effect on photosynthetic
614 performance or growth. *Plant Physiology* 147(1):115-127.
615 23. Tomaz T, *et al.* (2010) Mitochondrial malate dehydrogenase lowers leaf respiration and alters
616 photorespiration and plant growth in Arabidopsis. *Plant Physiology* 154(3):1143-1157.
617 24. Palmieri L, *et al.* (2008) Molecular identification of three *Arabidopsis thaliana* mitochondrial dicarboxylate
618 carrier isoforms: Organ distribution, bacterial expression, reconstitution into liposomes and functional
619 characterization. *The Biochemical journal* 410(3):621-629.
620 25. Picault N, Palmieri L, Pisano I, Hodges M, & Palmieri F (2002) Identification of a novel transporter for
621 dicarboxylates and tricarboxylates in plant mitochondria. Bacterial expression, reconstitution, functional
622 characterization, and tissue distribution. *The Journal of Biological Chemistry* 277(27):24204-24211.

- 623 26. Monné M, *et al.* (2018) Uncoupling proteins 1 and 2 (UCP1 and UCP2) from *Arabidopsis thaliana* are
624 mitochondrial transporters of aspartate, glutamate, and dicarboxylates. *Journal of Biological Chemistry*
625 293(11):4213-4227.
- 626 27. Wiskich JT (1977) Mitochondrial metabolite transport. *Annual Review of Plant Physiology* 28(1):45-69.
- 627 28. LaNoue KF & Schoolwerth AC (1979) Metabolite transport in mitochondria. *Annual Review of Biochemistry*
628 48(1):871-922.
- 629 29. Klingenberg M (1979) Overview on mitochondrial metabolite transport systems. *Methods in enzymology* 56:
630 245-252.
- 631 30. Van Aken O, *et al.* (2009) Defining the mitochondrial stress response in *Arabidopsis thaliana*. *Molecular*
632 *Plant* 2(6):1310-1324.
- 633 31. Senkler J, *et al.* (2017) The mitochondrial complexome of *Arabidopsis thaliana*. *The Plant Journal*
634 89(6):1079-1092.
- 635 32. Fuchs P, *et al.* (2020) Single organelle function and organization as estimated from *Arabidopsis*
636 mitochondrial proteomics. *The Plant Journal* 101(2):420-441.
- 637 33. Taylor NL, *et al.* (2014) Selected reaction monitoring to determine protein abundance in *Arabidopsis* using
638 the *Arabidopsis* Proteotypic Predictor. *Plant Physiology* 164(2):525-536.
- 639 34. Catoni E, *et al.* (2003) Identification of an *Arabidopsis* mitochondrial succinate–fumarate translocator. *FEBS*
640 *Letters* 534(1-3):87-92.
- 641 35. Tronconi MA, Maurino VG, Andreo CS, & Drincovich MF (2010) Three different and tissue-specific NAD-
642 malic enzymes generated by alternative subunit association in *Arabidopsis thaliana*. *Journal of Biological*
643 *Chemistry* 285(16):11870-11879.
- 644 36. Fahien LA, Kmietek EH, MacDonald MJ, Fibich B, & Mandic M (1988) Regulation of malate dehydrogenase
645 activity by glutamate, citrate, alpha-ketoglutarate, and multienzyme interaction. *Journal of Biological*
646 *Chemistry* 263(22):10687-10697.
- 647 37. Rawsthorne S & Hylton CM (1991) The relationship between the post-illumination CO₂ burst and glycine
648 metabolism in leaves of C₃ and C₃-C₄ intermediate species of *Moricandia*. *Planta* 186(1):122-126.
- 649 38. Wagner S, *et al.* (2019) Multiparametric real-time sensing of cytosolic physiology links hypoxia responses to
650 mitochondrial electron transport. *New Phytologist* 224(4):1668-1684.
- 651 39. Hung Yin P, Albeck John G, Tantama M, & Yellen G (2011) Imaging cytosolic NADH-NAD⁺ redox state with
652 a genetically encoded fluorescent biosensor. *Cell Metabolism* 14(4):545-554.
- 653 40. Gibon Y, *et al.* (2006) Integration of metabolite with transcript and enzyme activity profiling during diurnal
654 cycles in *Arabidopsis* rosettes. *Genome Biology* 7(8):R76.
- 655 41. Hildebrandt TM, Nunes-Nesi A, Araújo WL, & Braun H-P (2015) Amino acid catabolism in plants. *Molecular*
656 *Plant* 8(11):1563-1579.
- 657 42. Ishizaki K, *et al.* (2005) The critical role of *Arabidopsis* electron-transfer flavoprotein:ubiquinone
658 oxidoreductase during dark-induced starvation. *The Plant Cell* 17(9):2587-2600.
- 659 43. Peng C, Uygun S, Shiu S-H, & Last RL (2015) The impact of the branched-chain ketoacid dehydrogenase
660 complex on amino acid homeostasis in *Arabidopsis*. *Plant Physiology* 169(3):1807-1820.
- 661 44. Latimer S, *et al.* (2018) Metabolic reconstructions identify plant 3-methylglutaconyl-CoA hydratase that is
662 crucial for branched-chain amino acid catabolism in mitochondria. *The Plant Journal* 95(2):358-370.
- 663 45. Schertl P, Danne L, & Braun H-P (2017) 3-hydroxyisobutyrate dehydrogenase is involved in both, valine and
664 isoleucine degradation in *Arabidopsis thaliana*. *Plant Physiology* 175(1):51-61.
- 665 46. Ishizaki K, *et al.* (2006) The mitochondrial electron transfer flavoprotein complex is essential for survival of
666 *Arabidopsis* in extended darkness. *The Plant Journal* 47(5):751-760.
- 667 47. Araújo WL, *et al.* (2010) Identification of the 2-hydroxyglutarate and isovaleryl-CoA dehydrogenases as
668 alternative electron donors linking lysine catabolism to the electron transport chain of *Arabidopsis*
669 mitochondria. *The Plant Cell* 22(5):1549-1563.
- 670 48. Ding G, Che P, Ilarslan H, Wurtele ES, & Nikolau BJ (2012) Genetic dissection of methylcrotonyl CoA
671 carboxylase indicates a complex role for mitochondrial leucine catabolism during seed development and
672 germination. *The Plant Journal* 70(4):562-577.
- 673 49. Miyashita Y & Good AG (2008) NAD(H)-dependent glutamate dehydrogenase is essential for the survival of
674 *Arabidopsis thaliana* during dark-induced carbon starvation. *Journal of Experimental Botany* 59(3):667-680.
- 675 50. He Y & Gan S (2002) A gene encoding an acyl hydrolase is involved in leaf senescence in *Arabidopsis*. *The*
676 *Plant Cell* 14(4):805-815.
- 677 51. Miao Y & Zentgraf U (2007) The antagonist function of *Arabidopsis* WRKY53 and ESR/ESP in leaf
678 senescence is modulated by the jasmonic and salicylic acid equilibrium. *The Plant Cell* 19(3):819-830.
- 679 52. Oh SA, Lee SY, Chung IK, Lee C-H, & Nam HG (1996) A senescence-associated gene of *Arabidopsis*
680 *thaliana* is distinctively regulated during natural and artificially induced leaf senescence. *Plant Molecular*
681 *Biology* 30(4):739-754.

- 682 53. Pietrocola F, Galluzzi L, Bravo-San Pedro JM, Madeo F, & Kroemer G (2015) Acetyl coenzyme A: A central
683 metabolite and second messenger. *Cell Metabolism* 21(6):805-821.
- 684 54. Porcelli V, *et al.* (2018) Molecular identification and functional characterization of a novel glutamate
685 transporter in yeast and plant mitochondria. *Biochimica et Biophysica Acta (BBA) - Bioenergetics*
686 1859(11):1249-1258.
- 687 55. Masclaux-Daubresse C, *et al.* (2006) Glutamine synthetase-glutamate synthase pathway and glutamate
688 dehydrogenase play distinct roles in the sink-source nitrogen cycle in tobacco. *Plant Physiology* 140(2):444-
689 456.
- 690 56. Linka N & Weber APM (2010) Intracellular metabolite transporters in plants. *Molecular Plant* 3(1):21-53.
- 691 57. Selinski J & Scheibe R (2019) Malate valves: Old shuttles with new perspectives. *Plant Biology* 21(S1):21-
692 30.
- 693 58. Palmieri F, Pierri CL, De Grassi A, Nunes-Nesi A, & Fernie AR (2011) Evolution, structure and function of
694 mitochondrial carriers: A review with new insights. *The Plant Journal* 66(1):161-181.
- 695 59. Sweetlove LJ, Beard KF, Nunes-Nesi A, Fernie AR, & Ratcliffe RG (2010) Not just a circle: Flux modes in
696 the plant TCA cycle. *Trends in Plant Science* 15(8):462-470.
- 697 60. Fernie AR, Carrari F, & Sweetlove LJ (2004) Respiratory metabolism: Glycolysis, the TCA cycle and
698 mitochondrial electron transport. *Current Opinion in Plant Biology* 7(3):254-261.
- 699 61. Lee CP, *et al.* (2016) MSL1 is a mechanosensitive ion channel that dissipates mitochondrial membrane
700 potential and maintains redox homeostasis in mitochondria during abiotic stress. *The Plant Journal*
701 88(5):809-825.
- 702 62. Zhao Y, Yu H, Zhou J-M, Smith SM, & Li J (2020) Malate circulation: Linking chloroplast metabolism to
703 mitochondrial ROS. *Trends in Plant Science*. 25(5):446-454
- 704 63. Ashykhmina N, *et al.* (2019) PAPST2 plays critical roles in removing the stress signaling molecule 3'-
705 phosphoadenosine 5'-phosphate from the cytosol and its subsequent degradation in plastids and
706 mitochondria. *The Plant Cell* 31(1):231-249.
- 707 64. Gigolashvili T, *et al.* (2012) The Arabidopsis thylakoid ADP/ATP carrier TAAC has an additional role in
708 supplying plastidic phosphoadenosine 5'-phosphosulfate to the cytosol. *The Plant Cell* 24(10):4187-4204.
- 709 65. Fatland BL, Nikolau BJ, & Wurtele ES (2005) Reverse genetic characterization of cytosolic acetyl-CoA
710 generation by ATP-citrate lyase in Arabidopsis. *The Plant Cell* 17(1):182-203.
- 711 66. Gauthier PPG, *et al.* (2010) *In folio* isotopic tracing demonstrates that nitrogen assimilation into glutamate is
712 mostly independent from current CO₂ assimilation in illuminated leaves of *Brassica napus*. *New Phytologist*
713 185(4):988-999.
- 714 67. Journet EP & Douce R (1983) Mechanisms of citrate oxidation by percoll-purified mitochondria from potato
715 tuber. *Plant Physiology* 72(3):802-808.
- 716 68. He L, *et al.* (2019) Mitochondrial pyruvate carriers prevent cadmium toxicity by sustaining the TCA cycle and
717 glutathione synthesis. *Plant Physiology* 180(1):198-211.
- 718 69. Ohbayashi I, *et al.* (2019) Mitochondrial pyruvate dehydrogenase contributes to auxin-regulated organ
719 development. *Plant Physiology* 180(2):896-909.
- 720 70. Yu H, *et al.* (2012) A mutation in the E2 subunit of the mitochondrial pyruvate dehydrogenase complex in
721 Arabidopsis reduces plant organ size and enhances the accumulation of amino acids and intermediate
722 products of the TCA cycle. *Planta* 236(2):387-399.
- 723 71. Bao X, Focke M, Pollard M, & Ohlrogge J (2000) Understanding *in vivo* carbon precursor supply for fatty
724 acid synthesis in leaf tissue. *The Plant Journal* 22(1):39-50.
- 725 72. Smith SM, *et al.* (2004) Diurnal changes in the transcriptome encoding enzymes of starch metabolism
726 provide evidence for both transcriptional and posttranscriptional regulation of starch metabolism in
727 Arabidopsis leaves. *Plant Physiology* 136(1):2687-2699.
- 728 73. Gibon Y, *et al.* (2004) A robot-based platform to measure multiple enzyme activities in Arabidopsis using a
729 set of cycling assays: Comparison of changes of enzyme activities and transcript levels during diurnal cycles
730 and in prolonged darkness. *The Plant Cell* 16(12):3304-3325.
- 731 74. van der Graaff E, *et al.* (2006) Transcription analysis of Arabidopsis membrane transporters and hormone
732 pathways during developmental and induced leaf senescence. *Plant Physiology* 141(2):776-792.
- 733 75. Fan J, Yu L, & Xu C (2017) A central role for triacylglycerol in membrane lipid breakdown, fatty acid β -
734 oxidation, and plant survival under extended darkness. *Plant Physiology* 174(3):1517-1530.
- 735 76. Van Aken O, *et al.* (2016) Mitochondrial and chloroplast stress responses are modulated in distinct touch
736 and chemical inhibition phases. *Plant Physiology* 171(3):2150-2165.
- 737 77. Ghosh R, *et al.* (2016) Exposure to sound vibrations lead to transcriptomic, proteomic and hormonal changes
738 in Arabidopsis. *Scientific Reports* 6:33370.
- 739 78. Lin WD, *et al.* (2011) Coexpression-based clustering of Arabidopsis root genes predicts functional modules
740 in early phosphate deficiency signaling. *Plant Physiology* 155(3):1383-1402.

- 741 79. Lee D, Polisensky DH, & Braam J (2005) Genome-wide identification of touch- and darkness-regulated
742 Arabidopsis genes: A focus on calmodulin-like and XTH genes. *New Phytologist* 165(2):429-444.
- 743 80. Kilian J, *et al.* (2007) The ATGENEXPRESS global stress expression data set: Protocols, evaluation and
744 model data analysis of UV-B light, drought and cold stress responses. *The Plant Journal* 50(2):347-363.
- 745 81. Jander G & Joshi V (2009) Aspartate-derived amino acid biosynthesis in *Arabidopsis thaliana*. *Arabidopsis*
746 *Book 7*:e0121-e0121.
- 747 82. Li H, Hurlburt AJ, & Tennessen JM (2018) A Drosophila model of combined D-2- and L-2-hydroxyglutaric
748 aciduria reveals a mechanism linking mitochondrial citrate export with oncometabolite accumulation. *Disease*
749 *models & mechanisms* 11(9):dmm035337.
- 750 83. Mizuarai S, Miki S, Araki H, Takahashi K, & Kotani H (2005) Identification of dicarboxylate carrier SLC25A10
751 as malate transporter in *de novo* fatty acid synthesis. *Journal of Biological Chemistry* 280(37):32434-32441.
- 752 84. Li X, *et al.* (2017) LC-MS-based metabolomics revealed SLC25A22 as an essential regulator of aspartate-
753 derived amino acids and polyamines in KRAS-mutant colorectal cancer. *Oncotarget* 8(60):101333-101344.
- 754 85. Toka I, *et al.* (2010) Mutations in the hyperosmotic stress-responsive mitochondrial BASIC AMINO ACID
755 CARRIER2 enhance proline accumulation in Arabidopsis. *Plant Physiology* 152(4):1851-1862.
- 756 86. de Souza Chaves I, *et al.* (2019) The mitochondrial NAD⁺ transporter (NDT1) plays important roles in cellular
757 NAD⁺ homeostasis in *Arabidopsis thaliana*. *The Plant Journal* 100(3):487-504.
- 758 87. Feitosa-Araujo E, *et al.* (2020) Down-regulation of a mitochondrial NAD⁺ transporter (NDT2) alters seed
759 production and germination in Arabidopsis. *Plant and Cell Physiology*, pcaa017,
760 <https://doi.org/10.1093/pcp/pcaa017>
- 761 88. Kleinboelting N, Huep G, Kloetgen A, Viehoveer P, & Weisshaar B (2012) GABI-KAT simplesearch: New
762 features of the *Arabidopsis thaliana* T-DNA mutant database. *Nucleic Acids Research* 40(D1):D1211-D1215.
- 763 89. Lu Y, Savage LJ, Larson MD, Wilkerson CG, & Last RL (2011) Chloroplast 2010: A database for large-scale
764 phenotypic screening of Arabidopsis mutants. *Plant Physiology* 155(4):1589-1600.
- 765 90. Sweetlove LJ, Taylor NL, & Leaver CJ (2007) Isolation of intact, functional mitochondria from the model plant
766 *Arabidopsis thaliana*. *Mitochondria: Practical protocols*, eds Leister D & Herrmann JM (Humana Press,
767 Totowa, NJ), pp 125-136.
- 768 91. Lee CP, Eubel H, & Millar AH (2010) Diurnal changes in mitochondrial function reveal daily optimization of
769 light and dark respiratory metabolism in Arabidopsis. *Molecular & Cellular Proteomics* 9(10):2125-2139.
- 770 92. Huang S, Lee CP, & Millar AH (2015) Activity assay for plant mitochondrial enzymes. *Plant mitochondria:*
771 *Methods and protocols*, eds Whelan J & Murcha MW (Springer New York, New York, NY), pp 139-149.
- 772 93. Lee CP, Wirtz M, & Hell R (2014) Evidence for several cysteine transport mechanisms in the mitochondrial
773 membranes of *Arabidopsis thaliana*. *Plant and Cell Physiology* 55(1):64-73.
- 774 94. James AM, *et al.* (2019) The macrocyclizing protease butelase 1 remains autocatalytic and reveals the
775 structural basis for ligase activity. *The Plant Journal* 98(6):988-999.
- 776 95. Schwacke R, *et al.* (2003) ARAMEMNON, a novel database for Arabidopsis integral membrane proteins.
777 *Plant Physiology* 131(1):16-26.

778

779

780 **FIGURE LEGENDS**

781

782 **Figure 1. Phenotypic characterization of the *DIC2* mutant.** (A) Left, the gene model of *DIC2*
783 showing predicted transmembrane domains based on ARAMEMNON consensus prediction (95), the
784 position of T-DNA insertion in the *dic2-1* line and locations of peptides for LC-MRM-MS (in red lines)
785 and the transcript for qPCR (in green line). Middle, expression levels of *DIC2* as determined by qPCR
786 in different genotypes (n = 4). Right, LC-MRM-MS abundance analysis of unique peptides of *DIC2*
787 using the quantifier ion transitions VGPISLGINIVK and NYAGVGDAIR (n = 3). Mean \pm S.E., with
788 asterisks denote significant differences between *mcc-1* vs Col-0 and *mcc-1* vs *mcc-1/gMCC* based
789 on ANOVA and Tukey's post-hoc analysis (* p < 0.05; ** p < 0.01). (B) Vegetative phenotype of Col-
790 0, *dic2-1* and complemented lines (*gDIC2*, native promoter; *OE*, 35S promoter) grown on soil under
791 short day condition (8 h light/16 h dark) on 35, 42 and 49 days after germination. Representative top
792 view of various genotypes is shown. Expression levels are shown in Table S1.

793 **Figure 2. Uptake, consumption and export of TCA cycle intermediates by isolated**
794 **mitochondria.** (A) Experimental design for monitoring substrate consumption, product formation and
795 metabolite transport kinetics of isolated mitochondria. On the left, the mitochondrial TCA cycle and
796 pyruvate metabolising and generating steps are shown, along with the steps that generate reductants
797 for consumption by the ETC and the movements of organic acids across the membranes. Note that
798 the feeding substrate, which is in excess, could cause inhibition of specific steps of the TCA cycle
799 (e.g. feedback inhibition of citrate synthase by citrate). (i) Measurement of oxygen consumption by
800 substrate-fed mitochondria using Clarke-type oxygen electrode is an indirect assay for simultaneously
801 measuring substrate uptake and consumption and subsequent transfer of reductant to the ETC. (ii)
802 In a second approach, mitochondria are fed with a substrate under energised condition. After
803 indicated time interval, mitochondria are separated from extra-mitochondrial space by centrifugation
804 through a silicone oil layer. These fractions are collected, and substrates (S) and products (P) are
805 quantified by SRM-MS. (B) Bar graphs of V_{max} (upper panel) K_m (lower panel) for O_2 consumption in
806 the presence of substrate indicated. Mean \pm S.E. (n \geq 5). (C) Time-courses of pyruvate and/or OAA
807 concentrations in extra-mitochondrial space (i-iii) and the matrix (iv-vi) incubated with the indicated
808 feeding substrate. Mean \pm S.E. (n = 4). (D) [^{14}C]-malate uptake into isolated mitochondria as a function
809 of time under non-energising conditions. Isolated mitochondria were incubated in minimal transport
810 buffer containing 200 μ M malate without energising cofactors for the time indicated. Mean \pm S.E. (n
811 = 4). (E) Time-courses of fumarate concentrations in the extra-mitochondrial space (i-iii) and matrix
812 (iv-vi) incubated with the indicated feeding substrate. Mean \pm S.E. (n = 4). (G) Time-courses of citrate
813 concentrations in the extra-mitochondrial space (i-ii) and matrix (iii-iv) incubated with the indicated
814 feeding substrate. Mean \pm S.E. (n = 4). Asterisks denote significant differences between *mcc-1* vs

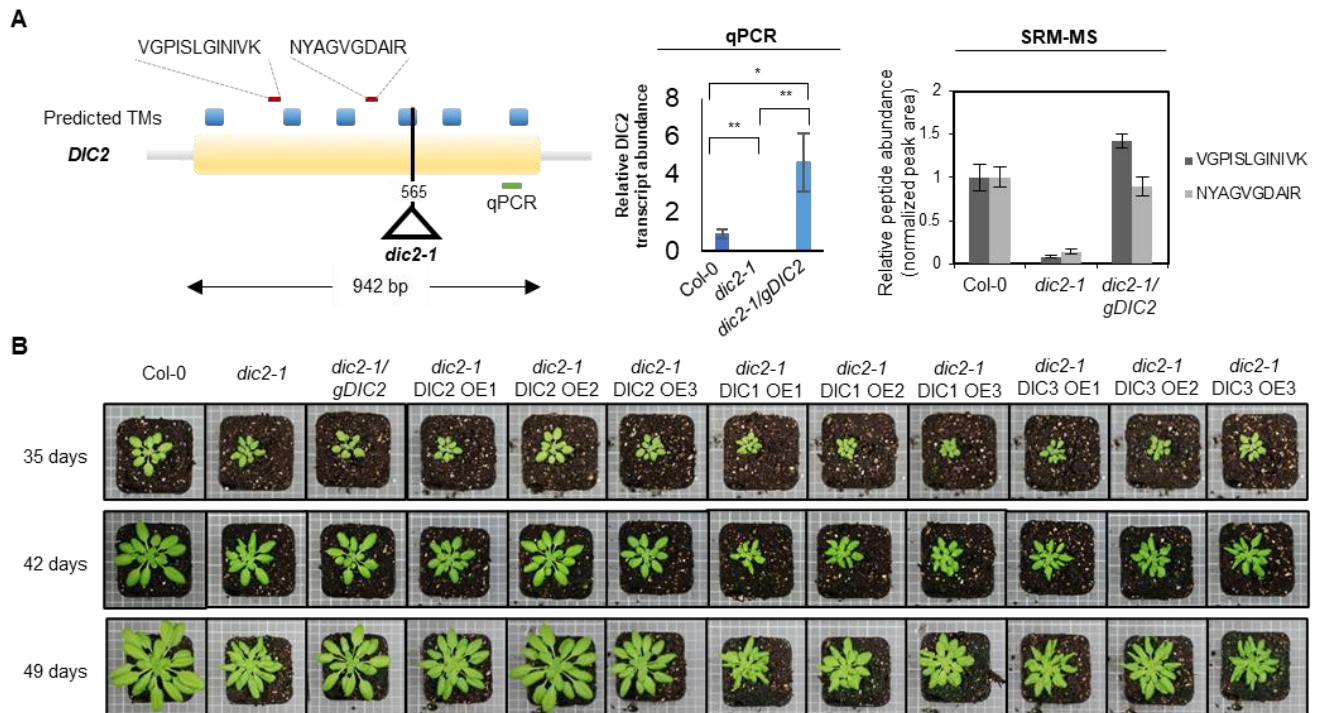
815 Col-0 and *mcc-1* vs *mcc-1/gMCC* based on ANOVA and Tukey's post-hoc analysis (* $p < 0.05$; ** $p <$
816 0.01). Response curves shown in C, E and F can also be found in Fig. S5.

817 **Figure 3. Photosynthetic and respiratory phenotypes of DIC2 knockout.** (A) Photosynthetic CO₂
818 assimilation rate at different photosynthetic active radiation (PAR) with CO₂ concentration at 400
819 p.p.m. and temperature at 22°C ($n = 6$, mean \pm S.E., no significant difference based on one-way
820 ANOVA). (B) Determination of post-illumination CO₂ burst. A single leaf illuminated with actinic light
821 of 1000 $\mu\text{mol m}^{-2} \text{s}^{-1}$, CO₂ concentration of 100 p.p.m. at 25°C was darkened for two minutes and
822 post-illumination burst was monitored in the first 30 s ($n = 6$, mean \pm S.E., data points within the
823 bracket indicate significant differences of $p < 0.05$ based on one-way ANOVA Tukey post-hoc test).
824 (C) Cytosolic NAD redox dynamics of 6-week-old leaves in response to a sudden light-to-dark
825 transition. Redox changes of the NAD pool correlate to the Peredox-mCherry ratio ($\log_{10}(\text{tS/mC})$), i.e.
826 high ratio indicates high NADH/NAD⁺ ratio. Dark adapted leaf discs were illuminated at actinic light of
827 220 $\mu\text{mol m}^{-2} \text{s}^{-1}$ according to *SI Methods* before they were transferred to the dark. The 5-min light/15-
828 min dark time course is shown on the left, with the red rectangle indicating the moment when
829 significant differences in NAD redox state were observed. Zoom-in of this red rectangle time interval
830 is shown on the right. Each data point represents mean \pm S.D. ($n \geq 6$), with asterisks indicate a
831 significant difference with $p < 0.001$ based on multiple t-tests ($\alpha = 5\%$) from the Holm-Sidak
832 Method. (D) Changes in the cytosolic NAD redox state over 8-h light/16-h dark diurnal cycle. Leaf
833 discs were exposed to actinic light of 120 $\mu\text{mol m}^{-2} \text{s}^{-1}$ before light was switched off. Two independent
834 lines (A and B) for each genotype were measured. Data shown indicate mean \pm SD ($n \geq 8$) with no
835 significant differences found between lines. (E) Time course of leaf respiration measurements in the
836 dark (R_N) as measured by Q2 ($n > 8$, mean \pm S.E., all time points are significantly difference with $p <$
837 0.05 based on one-way ANOVA Tukey post-hoc test). Response curves shown in C, E and F can
838 also be found in Fig. S5.

839 **Figure 4. Quantitative analysis of metabolites associated with the TCA cycle in a diurnal cycle**
840 **and during prolonged darkness.** (A) Plants were grown under short day conditions for 6 weeks and
841 leaf discs were collected at 1, 4, 8, 12 and 15 hours after dark shift and 1, 4 and 7 hours after light
842 shift. Metabolites in this figure were analysed by LC-MRM-MS. Metabolites are coloured according to
843 their accumulation pattern in *dic2-1* in a diurnal cycle: Orange, accumulates at night; Red,
844 accumulates during light and dark shift; Green, accumulates predominantly during the day; Blue,
845 accumulates throughout a diurnal cycle; Purple, accumulates only after the first hour of dark shift;
846 Grey, metabolite not measured. Each data point represents mean \pm S.E. ($n \geq 6$), asterisks indicate a
847 significant change as determined by the one-way ANOVA with Tukey post-hoc test (* $p < 0.05$; ** $p <$
848 0.01). (B) Heat map showing log₂-fold change, relative to Col-0, of TCA cycle intermediates, selected
849 amino acids and branched chain amino acid derivatives in four-week-old transgenic lines treated with
850 10 days of prolonged darkness ($n = 7$). BCKAs include: KIV, 2-oxoisovalerate; KIC, 2-oxoisocaproate;

851 KMV, 2-oxo-3-methylvalerate. * $p < 0.05$ and ** $p < 0.01$ according to the Student t-test. (C) Changes
852 in citrate, 2-OG and malate content in Arabidopsis plants after 0, 3, 7, 10 and 12 days of extended
853 darkness treatment ($n = 7$). Each data point represents mean \pm S.E. Asterisks indicate a significant
854 change as determined by one-way ANOVA with Tukey post-hoc test (* $p < 0.05$; ** $p < 0.01$).

855 **Figure 5. The loss of DIC2 causes an altered TCA cycle flux in the dark.** (A) Sucrose levels in
856 leaf discs from Col-0, *dic2-1* and *dic2-1/gDIC2* collected at different time points of a diurnal cycle (see
857 Figure 3 legend) as quantitatively determined by GC-MS against authentic standards ($n = 8$). (B)
858 qPCR analysis showing the expression of SEN1 in plants collected at the end of night (Shaded) or at
859 the end of day (Light). All expression values were normalised against Col-0 end of day sample ($n =$
860 4). (C) CO_2 evolution of leaf discs incubated in uniformly labelled ^{14}C -malate (left) and ^{14}C -leucine
861 (right) in the dark. $^{14}\text{CO}_2$ was captured in a NaOH trap, radiolabel in leaf discs was extracted and the
862 radioactivity in these samples were counted by a liquid scintillation counter. Data shown is the
863 percentage of CO_2 released relative to the total amount of radiolabel incorporated into leaf metabolism
864 ($n = 3$). (D) Schematic representation of all the possible incorporation patterns of isotope-labelled
865 glucose into the TCA cycle via pyruvate dehydrogenase and/or phosphoenolpyruvate (PEP)-OAA
866 interconversion in darkened leaf discs. Metabolites that were not measured are grey out. (E-F) Time-
867 courses of ^{13}C -labelling into metabolism in darkened leaf discs. Absolute abundance of total labelled
868 citrate (E, sum of m+2, m+3, m+4, m+5 and m+6), 2-oxoglutarate (F, sum of m+2, m+3, m+4 and
869 m+5), glutamine (G, sum of m+2, m+3, m+4 and m+5), threonine (H, sum of m+2 and m+4),
870 asparagine (I, sum of m+2 and m+4) and malate (J, sum of m+2 and m+4) are shown. Means \pm S.E.
871 ($n = 4$). Asterisks indicating significant differences (* $p < 0.05$; ** $p < 0.01$) as determined by one-way
872 ANOVA Tukey post-hoc analysis.



873

874

875

876

877

878

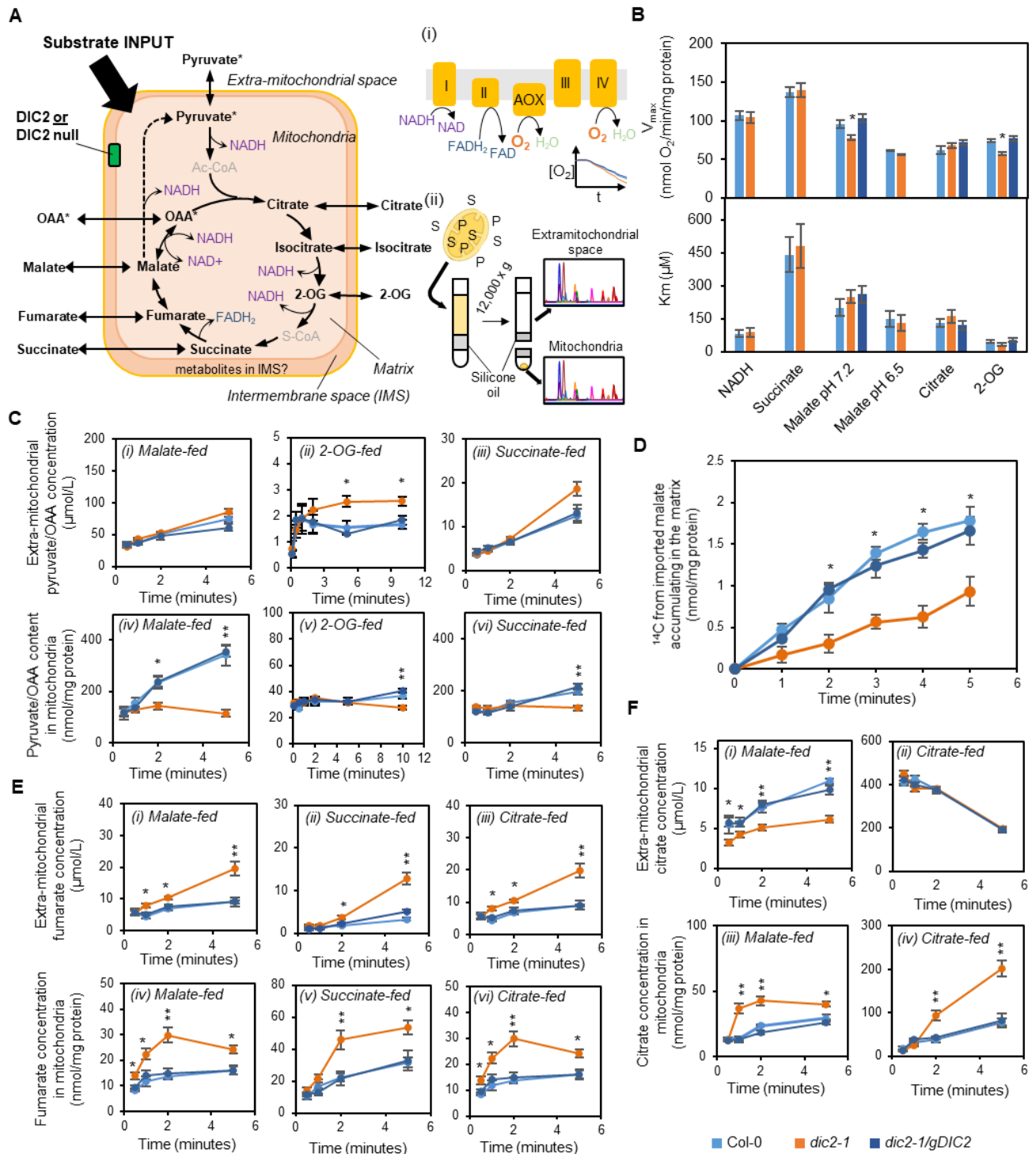
879

880

881

882

Figure 1. Phenotypic characterization of the *DIC2* mutant. (A) Left, the gene model of *DIC2* showing predicted transmembrane domains based on ARAMEMNON consensus prediction (95), the position of T-DNA insertion in the *dic2-1* line and locations of peptides for LC-MRM-MS (in red lines) and the transcript for qPCR (in green line). Middle, expression levels of *DIC2* as determined by qPCR in different genotypes ($n = 4$). Right, LC-MRM-MS abundance analysis of unique peptides of *DIC2* using the quantifier ion transitions VGPISLGINIVK and NYAGVGDAIR ($n = 3$). Mean \pm S.E., with asterisks denote significant differences between *mcc-1* vs Col-0 and *mcc-1* vs *mcc-1/gMCC* based on ANOVA and Tukey's post-hoc analysis (* $p < 0.05$; ** $p < 0.01$). (B) Vegetative phenotype of Col-0, *dic2-1* and complemented lines (*gDIC2*, native promoter; *OE*, 35S promoter) grown on soil under short day condition (8 h light/16 h dark) on 35, 42 and 49 days after germination. Representative top view of various genotypes is shown. Expression levels are shown in Table S1.



883

884

885

886

887

888

889

890

891

892

893

894

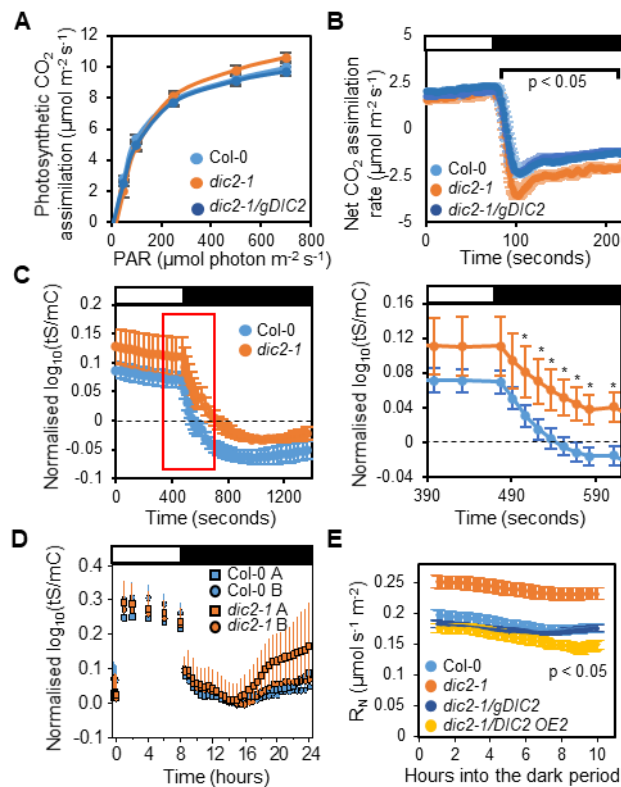
895

896

Figure 2. Uptake, consumption and export of TCA cycle intermediates by isolated mitochondria. (A) Experimental design for monitoring substrate consumption, product formation and metabolite transport kinetics of isolated mitochondria. On the left, the mitochondrial TCA cycle and pyruvate metabolising and generating steps are shown, along with the steps that generate reductants for consumption by the ETC and the movements of organic acids across the membranes. Note that the feeding substrate, which is in excess, could cause inhibition of specific steps of the TCA cycle (e.g. feedback inhibition of citrate synthase by citrate). (i) Measurement of oxygen consumption by substrate-fed mitochondria using Clarke-type oxygen electrode is an indirect assay for simultaneously measuring substrate uptake and consumption and subsequent transfer of reductant to the ETC. (ii) In a second approach, mitochondria are fed with a substrate under energised condition. After indicated time interval, mitochondria are separated from extra-mitochondrial space by centrifugation through a silicone oil layer. These fractions are collected, and substrates (S) and products (P) are quantified by SRM-MS. (B) Bar graphs of V_{max} (upper panel) K_m (lower panel) for O_2 consumption in the presence of substrate indicated. Mean \pm S.E. ($n \geq 5$). (C) Time-courses of pyruvate and/or OAA concentrations in extra-mitochondrial space (i-iii) and the matrix (iv-vi) incubated with the indicated feeding substrate. Mean \pm S.E. ($n = 4$). (D) [^{14}C]-malate uptake into isolated mitochondria as a function of time

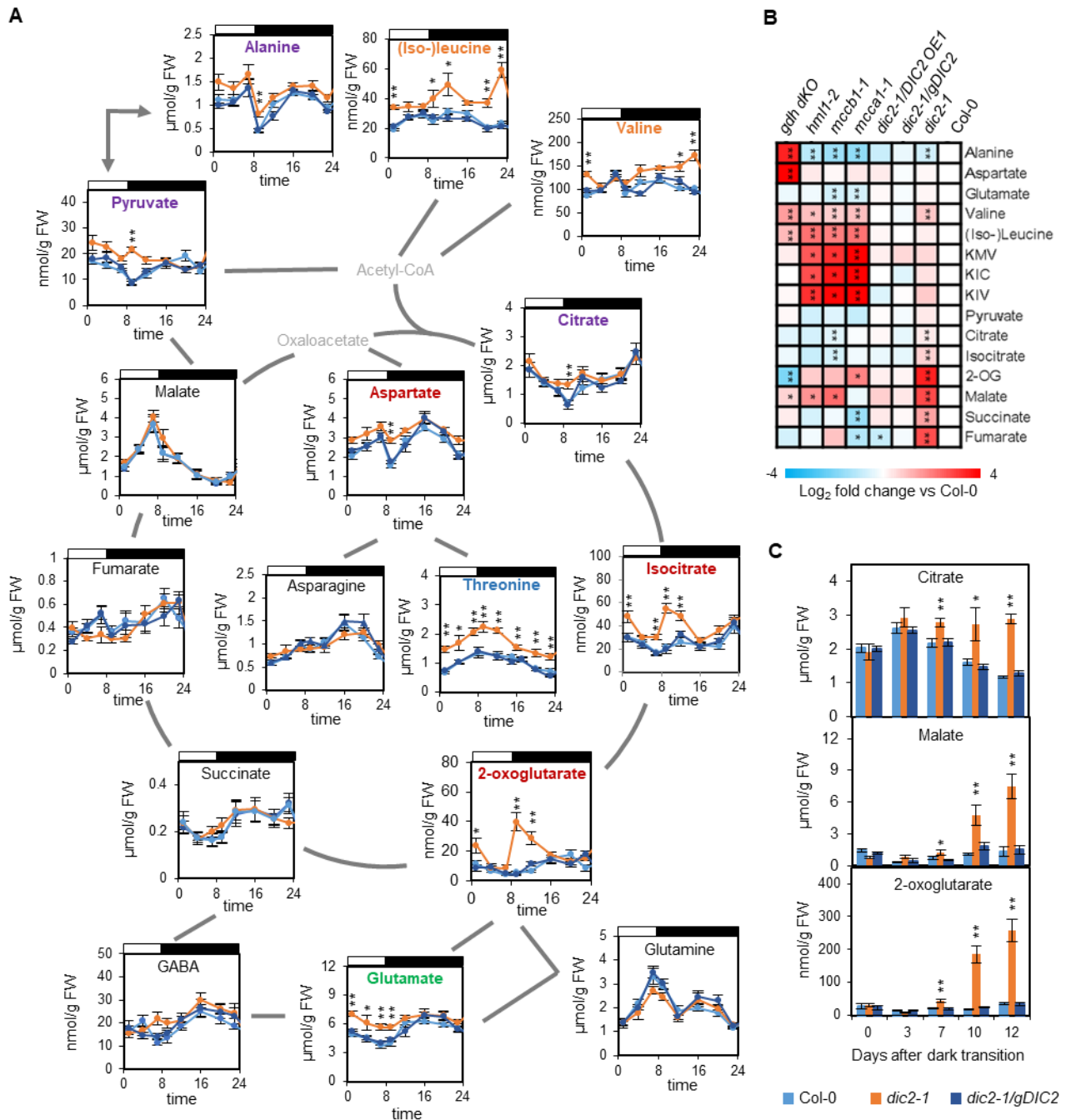
897 under non-energising conditions. Isolated mitochondria were incubated in minimal transport buffer containing 200 μ M malate
898 without energising cofactors for the time indicated. Mean \pm S.E. (n = 4). (E) Time-courses of fumarate concentrations in the
899 extra-mitochondrial space (i-iii) and matrix (iv-vi) incubated with the indicated feeding substrate. Mean \pm S.E. (n = 4). (G)
900 Time-courses of citrate concentrations in the extra-mitochondrial space (i-ii) and matrix (iii-iv) incubated with the indicated
901 feeding substrate. Mean \pm S.E. (n = 4). Asterisks denote significant differences between *mcc-1* vs Col-0 and *mcc-1* vs *mcc-*
902 *1/gMCC* based on ANOVA and Tukey's post-hoc analysis (* p < 0.05; ** p < 0.01). Response curves shown in C, E and F
903 can also be found in Fig. S5.

904

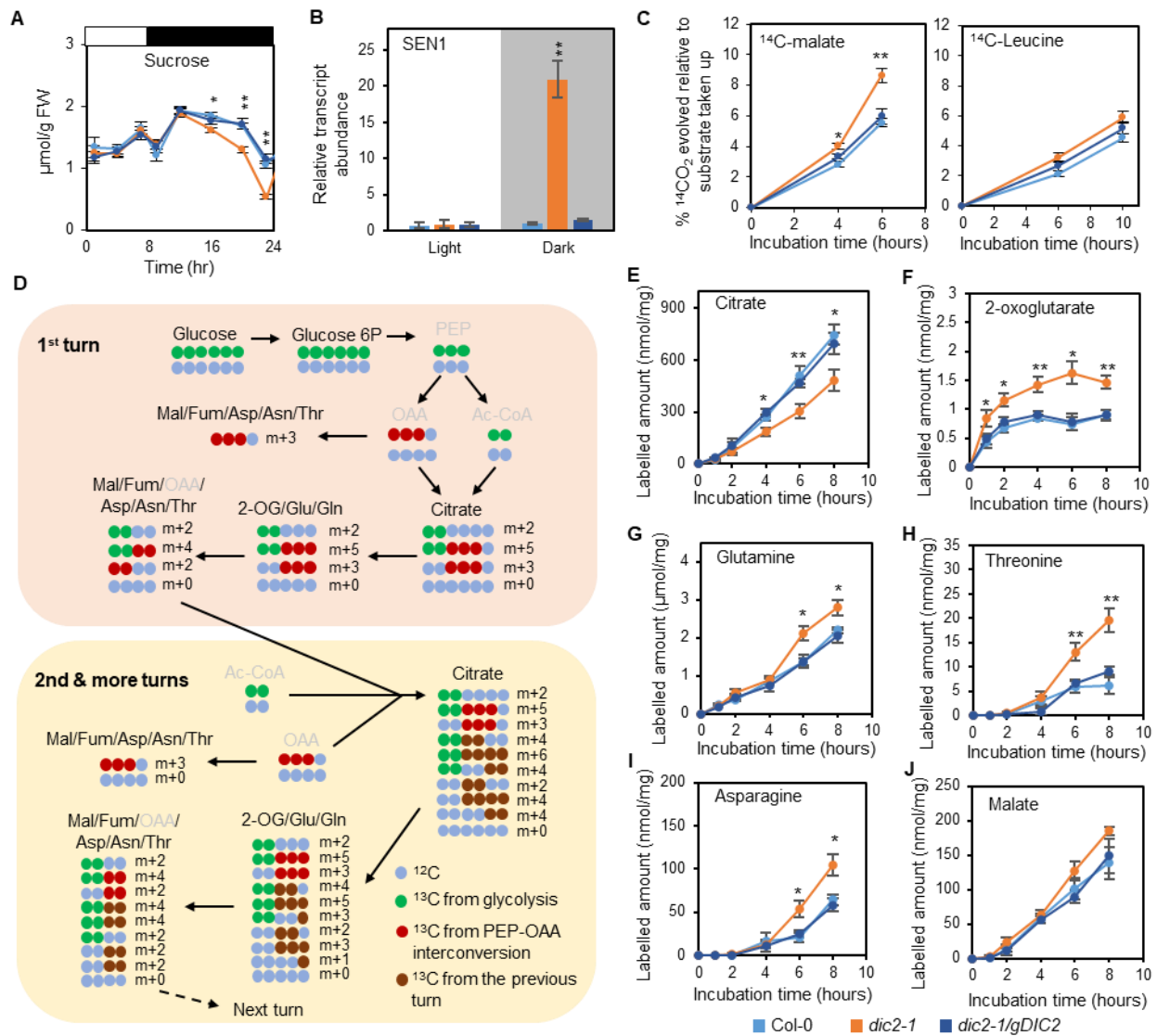


905

906 **Figure 3. Photosynthetic and respiratory phenotypes of DIC2 knockout.** (A) Photosynthetic CO₂ assimilation rate at
 907 different photosynthetic active radiation (PAR) with CO₂ concentration at 400 p.p.m. and temperature at 22°C (n = 6, mean
 908 ± S.E., no significant difference based on one-way ANOVA). (B) Determination of post-illumination CO₂ burst. A single leaf
 909 illuminated with actinic light of 1000 μmol m⁻² s⁻¹, CO₂ concentration of 100 p.p.m. at 25°C was darkened for two minutes
 910 and post-illumination burst was monitored in the first 30 s (n = 6, mean ± S.E., data points within the bracket indicate
 911 significant differences of p < 0.05 based on one-way ANOVA Tukey post-hoc test). (C) Cytosolic NAD redox dynamics of 6-
 912 week-old leaves in response to a sudden light-to-dark transition. Redox changes of the NAD pool correlate to the Peredox-
 913 mCherry ratio (log₁₀(tS/mC)), i.e. high ratio indicates high NADH/NAD⁺ ratio. Dark adapted leaf discs were illuminated at
 914 actinic light of 220 μmol m⁻² s⁻¹ according to *SI Methods* before they were transferred to the dark. The 5-min light/15-min
 915 dark time course is shown on the left, with the red rectangle indicating the moment when significant differences in NAD
 916 redox state were observed. Zoom-in of this red rectangle time interval is shown on the right. Each data point represents
 917 mean ± S.D. (n ≥ 6), with asterisks indicate a significant difference with p < 0.001 based on multiple t-tests (alpha = 5%)
 918 from the Holm-Sidak Method. (D) Changes in the cytosolic NAD redox state over 8-h light/16-h dark diurnal cycle. Leaf discs
 919 were exposed to actinic light of 120 μmol m⁻² s⁻¹ before light was switched off. Two independent lines (A and B) for each
 920 genotype were measured. Data shown indicate mean ± SD (n ≥ 8) with no significant differences found between lines. (E)
 921 Time course of leaf respiration measurements in the dark (R_N) as measured by Q2 (n > 8, mean ± S.E., all time points are
 922 significantly difference with p < 0.05 based on one-way ANOVA Tukey post-hoc test). Response curves shown in C, E and
 923 F can also be found in Fig. S5.



924
 925 **Figure 4. Quantitative analysis of metabolites associated with the TCA cycle in a diurnal cycle and during prolonged**
 926 **darkness.** (A) Plants were grown under short day conditions for 6 weeks and leaf discs were collected at 1, 4, 8, 12 and 15
 927 hours after dark shift and 1, 4 and 7 hours after light shift. Metabolites in this figure were analysed by LC-MRM-MS.
 928 Metabolites are coloured according to their accumulation pattern in *dic2-1* in a diurnal cycle: Orange, accumulates at night;
 929 Red, accumulates during light and dark shift; Green, accumulates predominantly during the day; Blue, accumulates
 930 throughout a diurnal cycle; Purple, accumulates only after the first hour of dark shift; Grey, metabolite not measured. Each
 931 data point represents mean \pm S.E. ($n \geq 6$), asterisks indicate a significant change as determined by the one-way ANOVA
 932 with Tukey post-hoc test (* $p < 0.05$; ** $p < 0.01$). (B) Heat map showing log₂-fold change, relative to *Col-0*, of TCA cycle
 933 intermediates, selected amino acids and branched chain amino acid derivatives in four-week-old transgenic lines treated
 934 with 10 days of prolonged darkness ($n = 7$). BCKAs include: KIV, 2-oxoisovalerate; KIC, 2-oxoisocaproate; KMV, 2-oxo-3-
 935 methylvalerate. * $p < 0.05$ and ** $p < 0.01$ according to the Student t-test. (C) Changes in citrate, 2-OG and malate content
 936 in *Arabidopsis* plants after 0, 3, 7, 10 and 12 days of extended darkness treatment ($n = 7$). Each data point represents mean
 937 \pm S.E. Asterisks indicate a significant change as determined by one-way ANOVA with Tukey post-hoc test (* $p < 0.05$; ** p
 938 < 0.01).



939

940 **Figure 5. The loss of DIC2 causes an altered TCA cycle flux in the dark.** (A) Sucrose levels in leaf discs from Col-0,
 941 *dic2-1* and *dic2-1/gDIC2* collected at different time points of a diurnal cycle (see Figure 3 legend) as quantitatively
 942 determined by GC-MS against authentic standards (n = 8). (B) qPCR analysis showing the expression of SEN1 in plants
 943 collected at the end of night (Shaded) or at the end of day (Light). All expression values were normalised against Col-0 end
 944 of day sample (n = 4). (C) CO₂ evolution of leaf discs incubated in uniformly labelled ¹⁴C-malate (left) and ¹⁴C-leucine (right)
 945 in the dark. ¹⁴CO₂ was captured in a NaOH trap, radiolabel in leaf discs was extracted and the radioactivity in these samples
 946 were counted by a liquid scintillation counter. Data shown is the percentage of CO₂ released relative to the total amount of
 947 radiolabel incorporated into leaf metabolism (n = 3). (D) Schematic representation of all the possible incorporation patterns
 948 of isotope-labelled glucose into the TCA cycle via pyruvate dehydrogenase and/or phosphoenolpyruvate (PEP)-OAA
 949 interconversion in darkened leaf discs. Metabolites that were not measured are greyed out. (E-F) Time-courses of ¹³C-
 950 labelling into metabolism in darkened leaf discs. Absolute abundance of total labelled citrate (E, sum of m+2, m+3, m+4,
 951 m+5 and m+6), 2-oxoglutarate (F, sum of m+2, m+3, m+4 and m+5), glutamine (G, sum of m+2, m+3, m+4 and m+5),
 952 threonine (H, sum of m+2 and m+4), asparagine (I, sum of m+2 and m+4) and malate (J, sum of m+2 and m+4) are shown.
 953 Means ± S.E. (n = 4). Asterisks indicating significant differences (* p < 0.05; ** p < 0.01) as determined by one-way ANOVA
 954 Tukey post-hoc analysis.